Engineering Journal issn: 0125-8281

Article

Effect of Extractant pH and Concentration of *Ageratum Conyziodes L* on the Optical Properties of Photosensitizer and Performance of Dye-Sensitized Solar Cell

Andhy Setiawan[1], **Sandi Muhammad Roziq**[1], **Eka Cahya Prima**[2,*], **Agus Danawan**[3], **Endi Suhendi**[1], **and Semuel Unwakoly**[2]

1 Physics Study Program, Faculty of Mathematics and Science Education, Universitas Pendidikan Indonesia, Bandung, Indonesia
2 Solar Energy Materials Laboratory, Department of Science Education, Faculty of Mathematics and Science Education, Universitas Pendidikan Indonesia, Bandung, Indonesia
3 Physics Education Study Program, Faculty of Mathematics and Science Education, Universitas Pendidikan Indonesia, Bandung, Indonesia
*E-mail: ekacahyaprima@upi.edu (Corresponding author)

Abstract. A dye-sensitized Solar Cell (DSSC) is a type of third-generation solar cell that uses dye as a light-sensitizing layer and is still under development. DSSC offers several advantages over previous generations, such as low production costs, simple manufacturing processes, and environmental friendliness, non-toxic and lightweight. However, in its development, natural dyes are derived from natural materials. This study focused on the optical properties and performance of DSSC as affected by variations in solvent pH and concentration of *Ageratum conyzoides L.* In this study, the pH of the solvent was varied at pH 1.00, 1.66, 2.27, and 3.00. Dye with solvent pH that has the best efficiency was then varied in concentration to 1.25gr/50ml, 2.5gr/50ml, 3.75gr/50ml, and 5gr/50ml. Fourier Transform Infrared (FTIR) characterization was used to identify the pigments contained in the dye. Raman spectroscopy, UV-Vis spectroscopy, cyclic voltammetry, electrochemical impedance spectroscopy, and J-V characteristic measurements were performed to analyze the optical properties and performance of the DSSC. The results showed that the dye sample in pH 1.00 solvent with 2,5gr/50ml concentration had the best performance with an average. $\overline{J_{sc}}$ $0.197\ mA/cm^2$, $\overline{V_{OC}}$ 0.525 V, $\overline{FF}$ 58.4%, and an average efficiency $\bar{\eta}$ 0.000598%. Although the DSSC in this study is less efficient than the typical efficiencies of 3-12% reported for natural dye-based DSSCs, this work highlights critical parameters such as solvent pH and dye concentration that influence performance. The results provide insights into addressing the inherent limitations of natural dyes in renewable energy applications, contributing to the ongoing advancements in environmentally friendly and sustainable solar energy technologies through the optimized use of natural dyes in DSSCs.

Keywords: Dye-sensitized solar cell, natural dye, renewable energy.

ENGINEERING JOURNAL Volume 29 Issue 4
Received 26 October 2024
Accepted 22 March 2025
Published 30 April 2025
Online at https://engj.org/
DOI:10.4186/ej.2025.29.4.1

1. Introduction

The increasing demand for sustainable energy solutions has driven the exploration of innovative technologies, and Dye-Sensitized Solar Cells (DSSCs) are emerging as a promising solution in renewable energy research [1]. In the past 20 years, there have been many studies on DSSCs as a cost-effective alternative energy source [2, 3]. Since their discovery in 1991 by Prof Gratzel, DSSCs have attracted the attention of many scientists due to their environmentally friendly nature and ease of fabrication [4]. The separation of light absorption and charge carrier transport functions is a technical differentiator of DSSCs from conventional semiconductor devices or photovoltaic solar cells [5].

Peng et al. [6] explain how DSSCs work: the light will pass through the transparent electrode and be absorbed by the photosensitizer (dye) to reach an excited state, and then the excited electrons will be projected into the conduction band of the semiconductor nanocrystal and transferred to the outer circuit. The electrons from the external circuit will pass through the counter electrode and replace the lost electrons in the electrolyte, as the redox couple will reduce the oxidized dye in the electrolyte to complete a cycle. In other words, DSSCs consist of a photoanode (working electrode), a counter electrode, a dye, and an electrolyte [7]. The photoanode is made using a transparent conductive substrate coated by semiconductor nanocrystals that bind to the photosensitizer (dye) [8]. Transparent conductive glass substrates commonly used for DSSC are Indium Tin Oxide or *ITO* and Fluorine-doped Tin Oxide or FTO [9]. The photoanode layer can be made using TiO_2, *ZnO*, and *SnO* semiconductor nanoparticles [10]. The return electrode is made from a platinum layer on a transparent conductive substrate [11]. Another important component is the electrolyte for dye reduction [8]. I^-/I_3^- electrolyte is a commonly used electrolyte in DSSC [12].

An issue found to be related to DSSCs is that dye selection has been shown to affect the overall efficiency of DSSCs greatly [13]. TiO_2 As a semiconductor material for DSSC photoanodes, it is widely used due to its wide band gap, lower conduction band than the energy level of the dye in the excited state, and good chemical stability [14, 15]. TiO_2 molecules have a porosity that allows dye molecules to attach. The light absorbed by the dye and its energy will be transferred in electrons by TiO_2 to the glass substrate [9]. When the dye pigment can absorb a wide range of light spectrum, the DSSC can produce higher efficiency. This makes the dye pigment a major player in DSSC [16]. In general, dyes as photosensitizers in DSSCs can be grouped into organic and inorganic [17]. Inorganic dyes generally consist of metal complexes such as ruthenium complexes and ruthenium-free dyes, while organic dyes consist of metal-free organic dyes and natural dyes [18]. Golshan et al. [19] stated that the best results of DSSCs using organic dyes and porphyrin-based dyes. Ruthenium-based DSSC with polypyridyl on TiO_2 nanocrystal semiconductor produces 11-12% efficiency. However, ruthenium is difficult to find, which makes it an expensive material [20]. Meanwhile, natural dyes have advantages such as good low-light performance and customizable integration of solar products and are in line with the mission of clean, renewable energy in manufacturing [21]. Natural dyes can be extracted more easily and are more environmentally friendly, making natural dyes the latest research in DSSCs [22]. Natural dye can be extracted from fruits, flowers, leaves, and other plant parts [17]. Dyes have an important role in DSSC productivity. Natural dyes that have been used are anthocyanins, chlorophyll, flavonoids, and carotin [23]. With all its advantages, DSSCs with natural dyes still produce low efficiency compared to other dyes [24]. Natural dyes from a mixture of two dye pigments, chlorophyll and anthocyanins, derived from Malva verticillata and Syzygium cumini plants obtained an efficiency of 1.84% [19]. Then, DSSC using natural persona derived from hard fruit produced an efficiency of 3.53% [25]. Calogero et al. [9] reported using red cabbage (Brassica oleracea), which produces anthocyanin pigments as a natural colorant for DSSC, with an efficiency of 2.90%. Raspberries and other berries produce 3.04% efficiency as DSSC natural colorants [3]. As a country with biodiversity, Indonesia has many plants that thrive, one of which is *bandotan* [26].

Bandotan (*Ageratum conyzoides L.*) is a wild plant that grows in plantations or fields [27]. In addition, bandotan can grow in various soil types and grows very quickly [28] Due to its availability, *bandotan* leaves have the opportunity to become a colorant for DSSC. Research conducted by Yadav et al. [29] suggested that *A. conyziodes L.* has a number of phytoconstituents in almost every part of the plant, such as alkaloids, flavonoids, terpenes, and sterols. As previously stated, flavonoids are one of the natural dyes that can be used as photosensitizers in DSSC.

Compared to other natural dyes, *Ageratum conyzoides L.* offers improved light-harvesting potential and stability under acidic conditions, as shown by its consistent absorbance and higher chlorophyll concentrations at lower pH levels. This stability under acidic conditions is advantageous for prolonging the operational life of DSSCs. The dual presence of flavonoids and chlorophyll also broadens the spectral range of light absorption, enhancing the dye's capacity to capture photons across a wider wavelength range. Collectively, these characteristics highlight the potential of Ageratum conyzoides L. to address known issues in DSSCs, such as limited absorption range and poor molecular stability, making it a valuable candidate for sustainable photovoltaic applications

In addition to dye selection as DSSC optimization, structural modification, search for new electrolytes, and modification of dye concentration can be done to optimize DSSC efficiency. According to Nasyori and Noor [30], one of the reasons for increasing DSSC efficiency is the high concentration of dye pigments. The

choice of solvent to extract the dye is the key to the performance of natural photosensitizers. Because natural dye pigments can undergo morphological changes due to the pH of the solvent [31]. Differences in solvent pH will affect the adsorption of dye pigments by the TiO_2 layer and have an impact on DSSC performance to a large extent [19, 32]. This happens because the pH of the solvent will change the molecular formation of the dye in its attachment to the TiO_2 molecule, the changed molecular formation will change the HOMO and LUMO of the dye. These changes will affect the transfer of electrons to the TiO_2 molecule [33, 34].

In this study, the synthesis and characterization of DSSC using natural dyes from *bandotan* leaf extract with different concentrations and solvent use will be carried out to find out how the concentration of *bandotan* leaf extract affects when used as a photosensitizer for DSSC.

Ageratum conyzoides L., commonly known as bandotan, stands out as a promising natural dye for DSSCs due to its rich phytochemical profile, which includes flavonoids and chlorophyll. These compounds are well-known for their ability to act as efficient photosensitizers. The FTIR analysis in this study confirmed the presence of key functional groups, such as hydroxyl (-OH), carbonyl (>C=O), and aromatic C=C bonds, which are critical for light absorption and electron transfer. The hydroxyl and carbonyl groups facilitate strong binding of dye molecules to the TiO_2 semiconductor surface, ensuring effective electron injection. Moreover, the UV-Vis spectroscopic results demonstrated that extracts of Ageratum conyzoides L. exhibit strong absorbance across the visible light spectrum, particularly in the 435–664 nm range, corresponding to chlorophyll and anthocyanin absorption peaks.

Compared to other natural dyes like red cabbage or anthocyanin-rich berries, Ageratum conyzoides L. offers improved light-harvesting potential and stability under acidic conditions, as shown by its consistent absorbance and higher chlorophyll concentrations at lower pH levels. This stability under acidic conditions is advantageous for prolonging the operational life of DSSCs. The dual presence of flavonoids and chlorophyll also broadens the spectral range of light absorption, enhancing the dye's capacity to capture photons across a wider wavelength range. Collectively, these characteristics highlight the potential of Ageratum conyzoides L. to address known issues in DSSCs, such as limited absorption range and poor molecular stability, making it a valuable candidate for sustainable photovoltaic applications.

Reproducibility is a critical challenge when working with natural dyes, given their inherent variability due to factors such as seasonal, regional, and environmental differences in the source material. To ensure reproducibility in this study, several measures were taken. First, the leaves of Ageratum conyzoides L. were collected from a single location (Arcamanik, Bandung City, Indonesia) to minimize regional variation. Second, all samples were harvested during the same season under similar climatic conditions, which helped control seasonal variability. Additionally, the extraction process was standardized by strictly following fixed parameters such as pH, temperature, maceration time, and solvent composition.

Despite the large number of investigations on DSSCs employing natural dyes, little is known about how solvent pH and extract concentration affect molecular structure, optical characteristics, and electron transfer efficiency. In order to enhance DSSC performance, this study optimizes the extraction parameters while exploring Ageratum conyzoides L. as a novel natural dye.

This study provides a systematic analysis of the effects of solvent pH and dye concentration on DSSC performance, which is less commonly explored in previous research. The use of *Ageratum conyzoides L.* as a dye source contributes novel insights into how its phytochemical profile (rich in flavonoids and chlorophyll) influences DSSC performance. Unlike studies focused solely on achieving high efficiency, this work offers foundational knowledge that can be applied to optimize extraction methods, dye stability, and energy level alignment in future research. By methodically altering these parameters, we offer fresh perspectives on how pH and concentration impact dye uptake, energy levels, and electron transport dynamics. By increasing the effectiveness of natural dyes through ideal extraction conditions, our research helps create sustainable and reasonably priced DSSCs.

2. Materials & Tools

The research method used was the experimental method. The independent variables used were solvent with varying acidity (pH) of 1.00, 1.66, 2.27, and 3.00, and concentration of bandotan leaves with solvent volumes of 1.25gr/50ml, 3.75gr/50ml, and 5gr/50ml.

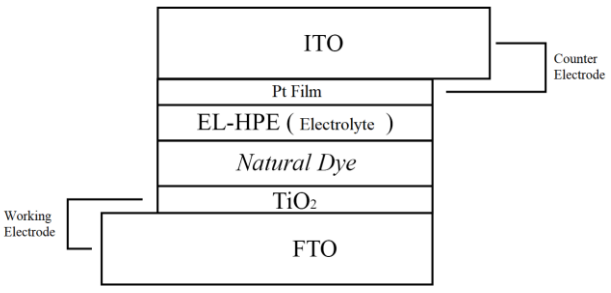

Fig. 1. DSSC layer structure.

The fixed variables used to control the study are the DSSC layer structure arranged like a sandwich with the configuration of $FTO/TiO_2/Dye/EL-HPE/Pt/ITO$ as shown in Fig. 1, and the dye from the bandotan leaf extract. The dependent variable to be obtained is the optical properties and performance of DSSC.

2.1. Materials

The materials used in this study were transparent conductive glass plate ITO; TiO_2 electrode (OPV-Tech, China), methanol (Merck, Germany), acetic acid (Merck, Germany), HCL (Merck, Germany), bandotan leaves picked from Arcamanik, Bandung City, Indonesia, 2-propanol (Merck, Germany), KNO_3 (Pundak Scientific, Indonesia), filter paper no. 102 (BKMAMLAB, China), distilled water, hexachloroplatinic acid (Sigma-Aldrich, Germany), EL-HPE/High-Performance Electrolyte (Greatcell, Australia), Low-Temperature Thermoplastic Sealant (Greatcell, Australia), dark glass bottle, aluminum foil, and cotton bud.

2.2. Tools

The tools used in this research are ultrasonic cleaner (BAKU BK-2000), drying oven (DHG-9053 A), muffle furnace (SUHATHERM), blender, and digital scales. Micropipette (Accurate), glass beaker, measuring cup, petri dish, Multimeter (KRISBOW KWD6-796), magnetic stirrer (DLAB MS-H260-Pro), spin coater (GLICHN T-108), Centrifuge (Oregon LC-04S), centrifuge tube, hair dryer, Filtration Buncher Vacuum Kit, pH meter (IONIX pH10), paper clip, Fourier Transform Infrared (BUNKER), UV-Vis spectrophotometer (W&J CE ROHS UV1600PC), DC Voltage Current Source/Monitor (ADCMT 6242), and Solar Standard Simulator AM 1.5G filter $100\ mW/cm^2$.

3. Procedures & Characteristics

3.1. Procedures

3.1.1. Dye extractrion

Firstly, 300 grams of bandotan leaves were washed and cleaned. After that, they were dried until there were no water droplets before being cut into smaller pieces. Then dried in a drying oven at 40°C for 24 hours. The temperature was chosen to resemble the condition when the leaves are dried under direct sunlight. After drying, the dried leaves were crushed into powder using a blender. On the other hand, we prepared several solutions that have different pH values. First, prepare methanol and acetic acid in a ratio of 95:5 (%v/v) with a total volume of 200 ml divided into four equally. After mixing them into a beaker, the solution was stirred using a magnetic stirrer at 1000 rpm at room temperature. To adjust the pH, we used hydrochloric acid (HCL). Each of the resulting solutions has a pH of 1.00, 1.66, 2.27, and 3.00 [34, 35, 36, 37].

The prepared fine powder was then dissolved into several solvents that had been made earlier in a ratio of 2.5gr/50ml (w/v). Then, the solution was stirred with a magnetic stirrer at 600 rpm for 2 hours. After the powder and solvent were stirred, the solution was macerated for 7 days at room temperature. After 7 days, the solution was ready for filtration using filter paper and a Filtration Buncher Vacuum Kit to speed up the process. After that, the solution was centrifuged at 4000 rpm for 10 minutes. The results were characterized, and the dye solution with the best absorbance was made in concentrations of 1.25gr/50ml, 3.75gr/50ml, and 5gr/50ml [38, 39, 40]

The maceration period of seven days was chosen to ensure maximum extraction of phytochemicals, such as flavonoids and chlorophyll, from Ageratum conyzoides L. This extended duration allows sufficient time for the solvent to penetrate the plant material and dissolve the desired pigments without degrading them. Prior studies, such as Hindryawati et al. [38], suggest that longer maceration times improve dye yield and enhance the optical properties of the extract.

The selected conditions—stirring speed of 600 rpm and a temperature of 40°C—were optimized based on their effectiveness in balancing efficient extraction and preventing thermal degradation of sensitive pigments. Stirring at 600 rpm ensures consistent mixing, maximizing the surface contact between the solvent and plant material, while the temperature of 40°C mimics natural drying under sunlight, maintaining the stability of temperature-sensitive compounds like chlorophyll and anthocyanins.

3.1.2. Photoanode synthesis

The TiO_2 coated FTO transparent conductive glass (TiO_2 electrode produced by OPVTech, China) was cleaned using an ultrasonic cleaner for 10 minutes. After that, they were heated at 80°C for 5 minutes before being immersed in each dye solution. Soaking was carried out for 3 days in a refrigerator, with the aim that the dye would not evaporate quickly due to its methanol content. After the immersion was complete, the photoanode was spelled with 2-propanol, and the part of the glass that was not coated with titania (TiO_2) was cleaned with a cotton bud and then allowed to dry.

3.1.3. Reverse electrode synthesis

ITO transparent conductive glass with a size of 1x2 cm was cleaned using an ultrasonic cleaner for 10 minutes. Then, the glass substrate was dried at 40°C for 5 minutes. The prepared glass was then treated with 25 µl of 20 mM hexachloroplatinic acid and spin-coated at 4000 rpm for 30 seconds. After that, the return electrode was heated to 80°C for 5 minutes. When the electrode temperature was equal to room temperature, the platinum electrode was burned at 350°C for 30 minutes.

3.1.4. DSSC fabrication

The fabricated photoanodes were arranged with reverse electrodes with both conductive sides in the center. Before joining, the photoanode was treated with Low-Temperature Thermoplastic Sealant around the TiO_2 thin film and EL-HPE electrolyte were then

dripped evenly over the TiO_2 film about 20 µl. The two electrodes were joined and clamped with a paper clip. Then, the DSSC was heated in an oven at 80°C for 5 minutes to melt the sealant so that the two electrodes adhered [41].

3.2. Characteristics

3.2.1. Characterisation of functional groups

Fourier transform infrared (FTIR) is a sample characterization that aims to determine the main functional groups that make up the sample molecule. This study used FTIR to determine the main groups that make up the dye molecule. Functional groups commonly found in dye pigments include hydroxyl (-OH), carboxylate (-COOH), carboxyl (>C=O), carbonyl (>C=C<), and methyl (-CH) [17].

3.2.2. Optical absorption characterisation

Characterization of the absorbance of dye-adsorbed TiO_2 and also dye was carried out using a UV-Vis spectrophotometer (W&J CE ROHS UV1600PC). This characterization aims to obtain the wavelength and absorbance values that this layer can absorb. These absorbance values were used to calculate the tested samples' LHE percentage and band gap values.

3.2.3. Characterisation of dye molecular energy levels

Cyclic voltammetry was used to determine the HOMO and LUMO energy levels of the dye. The characterization was carried out using three electrodes, where glassy carbon was used as the working electrode, platinum was used as the return electrode, and Ag/AgCl was used as the reference electrode. Then, the three electrodes were connected to a DC Voltage Current Source/Monitor to see the resulting graph of the dye solution with the electrolyte. The data generated is a current graph from -2 mV to +2 mV. The electrolyte solution used was 0.1M KNO_3 as much as 10 mL and was dripped with dye [19].

3.2.4. J-V characterization of DSSC

The characterization of J-V DSSC is done by connecting the two electrodes of DSSC to the DC Voltage Current Source/Monitor while being illuminated by Solar Standard Simulator 1.5 AM filter with $100\ mW/cm^2$ intensity. The characterization results will be processed to obtain data on short-circuit current density (J_{SC}), open-circuit voltage (V_{OC}), fill factor (FF), and DSSC efficiency (η).

4. Results & Discussions

4.1. Effect of Solvent pH on Photosensitizer Optical Properties and DSSC Performance

The chosen pH values for solvent extraction (1.00, 1.66, 2.27, and 3.00) were selected based on a combination of prior studies and preliminary experiments that highlighted the influence of pH on the stability and optical properties of natural dye extracts. Previous research, such as Al Qibtiya et al. [34] and Cahya Prima et al. [33], demonstrated that the acidity of the solvent plays a critical role in modulating the molecular structure of phytochemicals like chlorophyll and anthocyanins. Acidic conditions enhance the protonation of dye molecules, which can improve their adsorption onto the TiO_2 semiconductor surface and increase light absorption in certain wavelength ranges.

In this study, preliminary tests confirmed that pH values within the selected range significantly influenced the chlorophyll concentration and the dye's absorbance intensity, as evidenced by FTIR and UV-Vis results. These pH levels were also chosen to align with practical extraction methods while avoiding conditions that could degrade the dye's chemical structure. By systematically varying the pH, the study aimed to identify the optimal acidity for maximizing the dye's performance as a photosensitizer in DSSCs.

After A. Conyziodes L was extracted using a solution with solvent pH, Fourier transform infrared (FTIR) was performed to determine the functional groups that make up the dye molecule. FTIR results are shown as transmittance graphs at wave numbers 4000 to 500 cm^{-1} in Fig. 2.

From Fig. 2, it can be determined the functional groups that make up the dye molecule. It can be seen that there are 10-12 transmittance peaks owned by the dye and summarized in Table 1. The wide absorption peaks at wave numbers 3418 m^{-1}, 3400 m^{-1}, 3406 m^{-1}, and 3432 m^{-1} indicate absorption by hydroxyl (O-H) functional groups [42, 43, 44, 45]. Aliphatic C-H functional groups were seen at wave number 2950 m^{-1}, 2949 m^{-1}, 2948 m^{-1}, 2947 m^{-1} and 2842 m^{-1}, 2838 m^{-1}, 2839 m^{-1}, and 2848 m^{-1} [46, 47, 48, 49, 50, 51, 52, 53].

DOI:10.4186/ej.2025.29.4.1

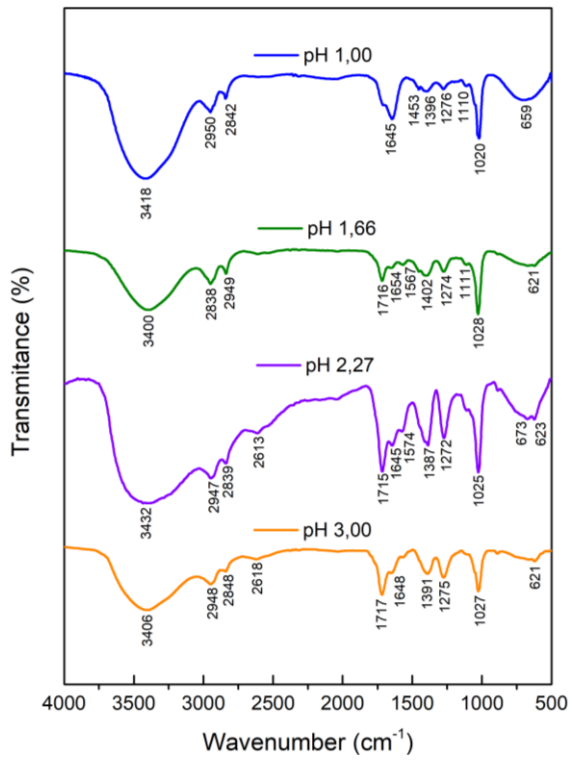

Fig. 2. FTIR Result.

Table 1. Identification and analysis of FTIR absorption peaks.

Wavenumber (m^{-1})				Functional Groups
pH 1,00	pH 1,66	pH 2,27	pH 3,00	
3418	3400	3406	3432	O-H Stretch
2950	2949	2948	2947	C-H alkane
2842	2838	2839	2848	
-	1716	1717	1715	C=O carboxyl
1645	1654	1645	1648	C=C aromatic
	1567	1574		
1453	1402	1387	1391	C-H alkane
1396				
1276	1274	1272	1276	C-O
1110	1110			
1020	1028	1025	1027	C-N
659	621	673	621	C-H Bending
		623		

At wave number 1716 m^{-1}, 1717 m^{-1}, and 1715 m^{-1} there are absorption peaks from double bonds of carboxyl (C=O) functional groups, which can be derived from carboxylic acids, ketones, or aldehydes [54, 55, 56]. Stretching at the double bond of the aromatic ring (aromatic C=C) was found at wave numbers 1645 m^{-1}, 1654 m^{-1}, 1648 m^{-1}, 1575 m^{-1}, and 1574 m^{-1} [57, 58, 59, 60]. These aromatic rings are usually responsible for the delivery of delocalized π electrons, which are later excited to LUMO and become the DSSC electric current [61, 62]. At wavelengths of 1387 m^{-1}, 1391 m^{-1}, 1396 m^{-1}, 1402 m^{-1}, and 1453 m^{-1} there is absorption by C-H bonds also from alkanes [8, 16, 19, 63]. There are functional groups showing C-N at 1020 m^{-1}, 1025 m^{-1}, 1027 m^{-1}, and 1028 m^{-1} [64, 65, 66, 67]. C-O functional groups are seen to appear mainly at the absorption peaks of 1110 m^{-1}, 1272 m^{-1}, 1274 m^{-1}, and 1276 m^{-1} [68, 69, 70, 71]. Finally, in the fingerprint region, the C-H bending functional group vibrates at wave number 621 m^{-1}, 659 m^{-1}, and 673 m^{-1} [72, 73].

Based on FTIR analysis and other scientific studies, these A. Conyziodes leaves contain flavonoids and chlorophyll. The structure of this flavonoid compound is indicated by the presence of functional groups such as O-H, aromatic C-H, C=O, and aromatic C=C in accordance with the FTIR spectrum [65]. Meanwhile, the real structure of chlorophyll is indicated by the presence of functional groups such as C-H, C=O, C=C, C-O, and C-N [74, 75]. The more acidic environment affects the shift in absorption peaks and intensity, and raises or eliminates functional groups [76].

The FTIR analysis revealed the presence of key functional groups such as hydroxyl (-OH) and carbonyl (>C=O) in the Ageratum conyzoides L. extract. These groups play a dual role in influencing the performance of DSSCs. The hydroxyl (-OH) and carbonyl (>C=O) groups act as anchoring sites that enable the dye molecules to bind strongly to the TiO_2 surface. This ensures better electron injection from the excited dye molecules into the TiO_2 conduction band, improving the overall photocurrent. These groups contribute to the dye's ability to absorb light by extending conjugation within the molecule, which helps in capturing photons more effectively across the visible spectrum. Moreover, The aromatic structure associated with these functional groups facilitates electron delocalization, enhancing the efficiency of electron transfer upon excitation. However, the presence of hydroxyl groups can promote hydrogen bonding between dye molecules, leading to aggregation on the TiO_2 surface. This reduces the active sites available for light absorption and hinders efficient electron injection. If the dye molecules are not uniformly bound to the TiO_2, the hydroxyl and carbonyl groups may lead to uneven electron injection or increased recombination rates, where electrons recombine with the oxidized dye or redox couple before contributing to the current.vThe hydroxyl groups, in particular, can be prone to degradation under prolonged light exposure or in less stable environments, reducing the dye's long-term efficiency.

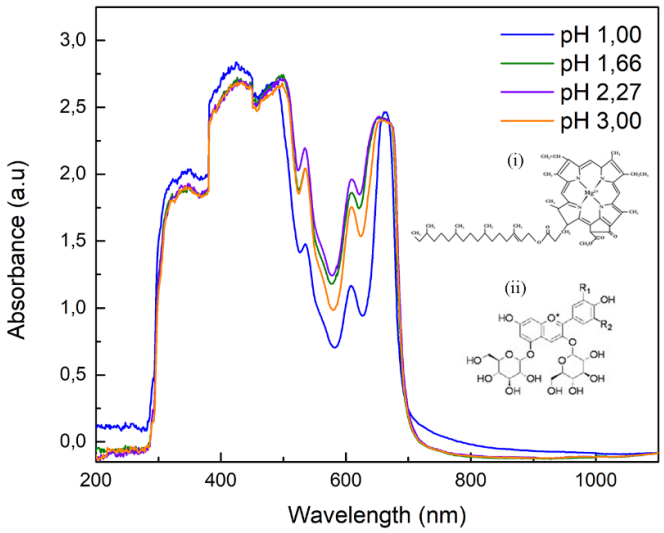

Fig. 3. UV-Vis absorption spectra of dye with solvent pH, inset: (i) chlorophyll A; and (ii) cyanidin 3,5 diglucoside.

Lastly, hydroxyl and carbonyl groups enhance binding and light absorption, their tendency to promote aggregation and recombination limits the performance of DSSCs. Addressing these limitations through strategies like dye co-sensitization or surface modifications on TiO_2 could further optimize the efficiency of DSSCs using natural dyes.

In the absorbance test using a UV-Vis Spectrophotometer, it can be seen that each dye has a relatively similar absorption area and peak, as shown in Fig. 3. The results of extraction with different pH solvents in A. Conyziodes L has an optimal absorption area at a wavelength of 800-300 nm; absorption rises at a wavelength range of 300-500 nm, then there is a fluctuation of absorption in the range of 500-650 nm, and rises again in the range of 650-800 nm. The condition of maximum absorption also indicates the stability of the dye molecules under light exposure. A stable absorption peak ensures consistent performance over time, which is crucial for practical applications. This shows that two phytoconstituents based on the pattern and absorption peaks support the IR results. The presence of chlorophyll A is shown in the absorption peak of 435-500 nm in the soret band and 653-664 nm in the Q band [75], while in the range of 500-650 nm shows the anthocyanin pattern in the flavonoid group called cyanidin 3,5 diglucoside which has a peak of 535-537 nm [77].

Table 2. Effect of extracting pH on chlorophyll A concentration.

pH	λ Soret band chlorophyll A (nm)	Chlorophyll A concentration (mM)	λ Q band chlorophyll A (nm)
3,00	435	24,1	658
2,27	500	24,4	653
1,66	494	24,6	658
1,00	424	25,4	661

Table 3. Effect of extracting pH on Cyanidin 3,5-diglucoside concentration.

pH	λ Cyanidin 3,5 - diglucoside (nm)	Cyanidin 3,5 - diglucoside concentration (mM)
3,00	535	76,1
2,27	534	81,6
1,66	535	75,9
1,00	537	54,4

A decrease in pH to a more acidic level affects the decrease in cyanidin 3,5 diglucoside concentration and increases the chlorophyll A content shown in Table 2 and Table 3. The absorption peaks of all samples are in the soret band region of chlorophyll. The increase in chlorophyll concentration is indicated by the increase in absorbance intensity in the sorbet band region (300-500 nm), where pH 1.00 has the largest absorbance with an absorption peak at 435 nm. As the pH increased to more alkaline conditions resulted in a decrease in the absorbance peak, which correlated to a decrease in chlorophyll concentration, the order of absorbance peak $A_{Max\ pH\ 1.00} > A_{Max\ pH\ 1.66} > A_{Max\ pH\ 2.27} > A_{Max\ pH\ 3.00}$. While in the Q band (650-800 nm) still shows, the dye solvent that has a pH of 1.00 is the largest absorbance intensity, but in the next order, followed by pH 2.27 with an absorbance intensity value of 2.43 a.u, and in the last order is a solvent with a pH of 3.00. Research conducted by [78] resulted in the same effect on chlorophyll. Where an increase in acidity impacts increasing intensity, increasing the number of hydrogen bonds in acidic conditions supports the formation of aggregates, which affect the photophysical properties of molecules. The effect of cyanidin 3,5 diglucoside was seen in the range of 500-650 nm. The decrease in pH shows the reverse for cyanidin 3.5 diglucoside compared to chlorophyll A. The concentration of these types of anthocyanins in the pH 1.00 solvent has the smallest absorbance intensity with an absorption peak at 537 nm, and the largest absorbance intensity belongs to pH 2.27 with an absorbance intensity value of 2.20 a.u at an absorption peak of 534 nm. The decrease in pH has an impact on the decrease in anthocyanin intensity peak. This was also experienced by Mejica et al. [79] when examining DSSC using Basella alba, the absorption weakened as the pH decreased from the neutral pH.

Rápó and Tonk [80] explained that when the pH is low, the dye molecule undergoes protonation, which causes changes in the electron structure and causes the dye's ability to absorb light at certain wavelengths to decrease.

The UV-Vis results in this study revealed variations in absorbance across different pH levels of the solvent, showing notable trends in the visible spectrum. These trends are closely tied to the molecular-level interactions between the dye molecules and the TiO_2 semiconductor surface. At lower pH (e.g., pH 1.00), the UV-Vis spectra showed stronger absorbance peaks, particularly in regions associated with chlorophyll and anthocyanins. Acidic conditions promote protonation of the dye molecules, which stabilizes the chlorophyll structure and enhances its light absorption. This was evident in the increased intensity of the soret and Q bands (435–664 nm). Conversely, at higher pH values (e.g., pH 3.00), the absorbance intensity decreased, reflecting changes in the dye's molecular structure. Alkaline conditions may reduce the stability of key pigments or alter their ability to bind effectively to the TiO_2 surface.

Functional groups in the dye molecules, such as hydroxyl (-OH) and carbonyl (>C=O), interact with the TiO_2 surface through coordination bonds. The UV-Vis results suggest that pH affects the availability and orientation of these groups, influencing how the dye molecules bind to TiO_2. For example, stronger absorbance at acidic pH indicates better molecular alignment and surface coverage. At lower pH, the enhanced absorbance corresponds to a higher population of excited electrons, which can be efficiently injected into the TiO_2 conduction band. This aligns with the observed narrowing of the dye's bandgap (e.g., 1.62 eV at pH 1.00), which facilitates better electron transfer.

UV-Vis data also reflect molecular interactions like aggregation, which increases at extreme pH levels. For instance, higher absorbance intensity at acidic pH could indicate the formation of aggregates, which, while enhancing light absorption, might limit efficient electron injection due to reduced interaction with the TiO_2 surface.

The trends observed in UV-Vis results highlight the importance of controlling solvent pH to achieve an optimal balance between maximizing light absorption and minimizing aggregation. The molecular-level interactions indicated by the absorption data suggest that acidic conditions enhance the dye's compatibility with TiO_2, improving its role as a photosensitizer.

The UV-Vis absorbance trends demonstrate how pH influences the molecular structure and binding properties of the dye, which in turn affect its interaction with TiO_2. Lower pH enhances dye adsorption and electron injection, while higher pH may reduce efficiency by destabilizing key pigments or weakening dye-TiO_2 interactions. These findings underline the critical role of solvent pH in optimizing DSSC performance.

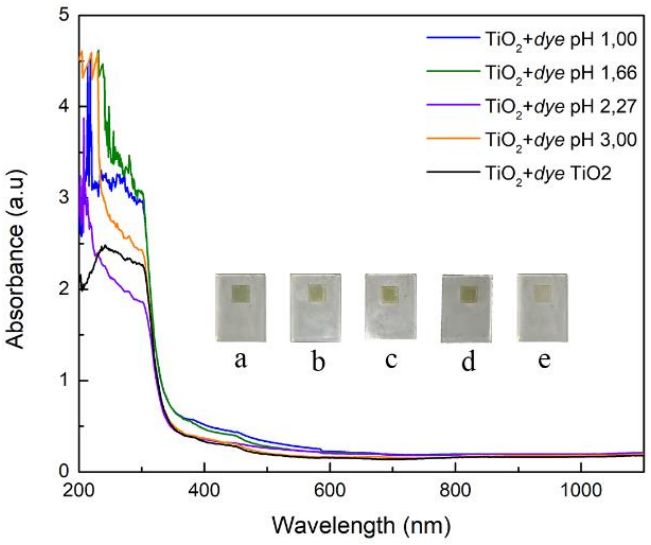

Fig. 4. UV-Vis Spectrometry graph of TiO_2+Dye with respect to solution pH (i) and UV-Vis Spectrometry graph of TiO_2+Dye with respect to solution pH in the 300-800 nm range (ii), inset: dye-stained TiO_2 samples with solvent pH 1.00 (a), pH 1.66 (b), pH 2.27 (c), pH 3.00 (d), and standard TiO_2photoanode (e).

The spectrograph results on the TiO_2 The layer that has been colored in Fig. 4 shows an expansion of the absorbance region caused by an increase in the intensity of visible and ultraviolet light. This shows that the dye is able to increase the range of light absorption that TiO_2 is not able to absorb. In the range of 380-700 nm (visible light), the effect of solvent pH on the dye is still the same, with an impact on increasing intensity. TiO_2 that has been bound with dye in that range shows pH 1.00 has the highest absorbance intensity compared to other results. Giving acid to the solvent results in an increase in the absorption area, which is characterized by increased intensity. While the absorption peak in the ultraviolet range (200-380 nm) is different from visible light. Dye with pH 1.66 solvent that binds to TiO_2 has the most considerable absorbance value, which is 4.62 a.u at a wavelength of 231 nm. The next order of absorbance peak is pH 3.00 with 4.61 a.u at a wavelength of 205 nm, then pH 1.00 with 4.54 a.u at a wavelength of 218 nm, and the smallest absorbance peak pH 2.27 with 4.59 a.u at a wavelength of 231 nm. Yadav et al. [25] reported that the surface of TiO_2 adsorbed by dye molecules increased in intensity. Just like the research conducted by Pratiwi et al. [81] there is an increase in the absorption spectrum of TiO_2 thin films in the visible light range, which means that the application of dye to the TiO_2 surface can be used as a photosensitizer for DSSC absorption in this range.

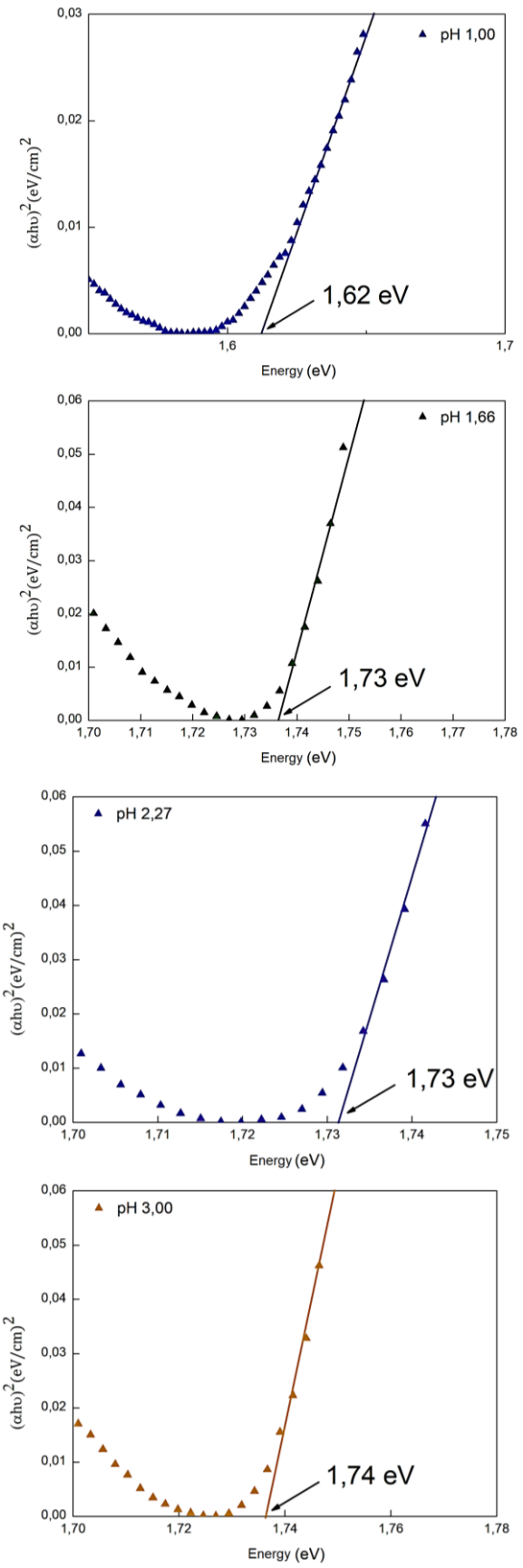

Fig. 5. Tauc's plot of dye samples with pH of solvent.

From the UV-Vis absorption data on the dye, the band gap value of each dye is obtained from the Tauc-s Plot analysis with the value of $(\alpha hv)^2$ on the y-axis against the energy value (eV) on the x-axis, as in Fig. 5 [82]. By drawing a line tangent to the graph and intersecting with the x-axis, the band gap values of 1.62 eV, 1.73 eV, 1.73 eV, and 1.74 eV are obtained for pH 1.00, pH 1.66, pH 2.27, and pH 3.00 respectively. The reduction in band gap value is caused by a decrease in pH in a more acidic environment [17]. This occurs because changes in the pH of the solvent result in changes in the molecular structure of the dye constituent, such as breaking some of the dye molecular bond chains. DSSC research using papaya leaves and pH as a solvent variation showed that the band gap decreased as the pH of the solvent decreased [83].

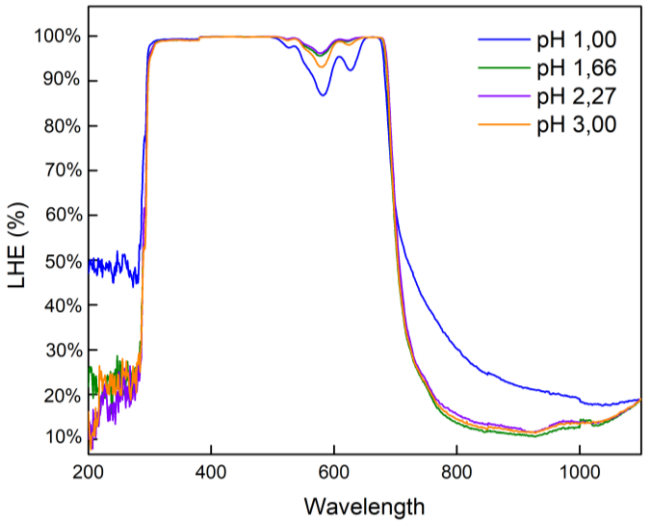

Fig. 6. Percentage of Light Harvesting Efficiency (LHE) of dye samples with solvent pH.

A graph of the percentage of Light Harvesting Efficiency (LHE) of each dye sample is shown in Fig. 6. Solvent pH affects the percentage of LHE peak, the more acidic the solvent, the higher the LHE peak. However, if the results of the pH of the solvent, the LHE percentage value is averaged, the highest LHE percentage average value of 40.7% is obtained, followed by pH 2.27 of 31.1% and pH 1.66 with an average LHE of 30.7%. While the lowest LHE average is a dye with a pH 3.00 solvent of 30.6%. One of the critical factors of DSSC performance is this LHE value.

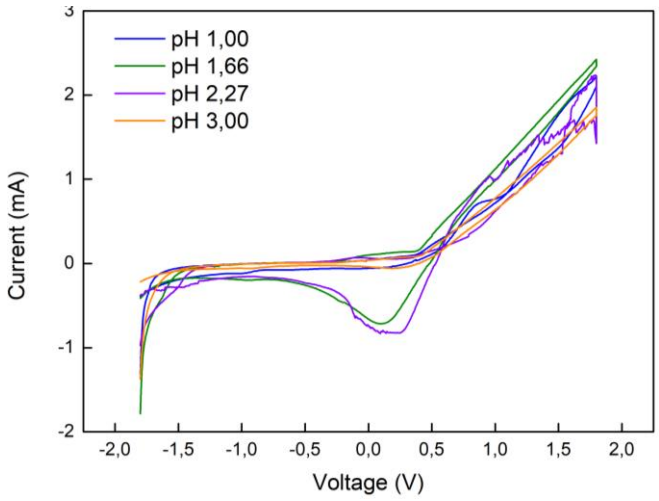

Fig. 7. Cyclic Voltammetry graph of dye sample with solvent pH.

To determine the voltage when oxidation occurs in the dye using Cyclic Voltammetry. The graph of CV reading results is shown in Fig. 7. The Lower Unoccupied Molecular Orbital (LUMO) value is obtained by reducing the band gap energy value with the HOMO value. The oxidation energy (E_{oks}) the analysis results are 0.41 V for pH 1.00, 0.34 for pH 1.66, 0.36 V for pH 2.27, and 0.37 V for pH 3.00. This oxidation energy is then used to determine the HOMO energy level in the dye, as shown in Table 4.

The cyclic voltammetry (CV) data provided valuable insights into the HOMO (highest occupied molecular orbital) and LUMO (lowest unoccupied molecular orbital) energy levels of the dye extracted from Ageratum conyzoides L. These levels are critical in determining the efficiency of electron injection into the TiO_2 conduction band and the regeneration of the oxidized dye by the iodine/iodide redox couple.

The conduction band of TiO_2 is typically located around -4.0 eV (vs. vacuum). In this study, the LUMO energy levels of the dye ranged from -3.01 eV to -3.20 eV (depending on the solvent pH). This difference indicates that the energy gap between the dye's LUMO and TiO_2 conduction band is relatively narrow. While this allows for electron injection, the smaller energy difference may limit the driving force for efficient electron transfer, potentially explaining the low photocurrent (Jsc) observed.

The iodine/iodide redox potential is approximately -4.8 eV (vs. vacuum). The HOMO energy levels of the dye ranged from -4.74 eV to -5.21 eV. These values show that the dye's HOMO is well-aligned with the redox couple, enabling effective regeneration of the oxidized dye. However, the deeper HOMO level at pH 1.00 (-5.21 eV) could increase the energy barrier for dye regeneration, slightly affecting the redox cycle efficiency.

The energy level alignment partially explains the observed low efficiency (0.000598%). While the HOMO and LUMO levels support basic dye functionality, the narrow energy difference between the LUMO and the TiO_2 conduction band reduces the efficiency of electron injection. Additionally, a deeper HOMO level, though beneficial for avoiding recombination, may slow down the dye regeneration process, contributing to performance losses.

Furthermore, suboptimal alignment can exacerbate recombination losses and reduce the effectiveness of the light-harvesting process, despite the observed high light-harvesting efficiency (LHE).

The HOMO and LUMO energy levels of the dye are moderately aligned with the TiO_2 conduction band and iodine/iodide redox couple, enabling basic DSSC operation but limiting overall efficiency. Addressing this limitation through dye engineering (e.g., tuning energy levels via co-sensitization or modifying functional groups) could enhance the driving forces for electron injection and dye regeneration, thereby improving device performance.

Table 4. Electrochemical parameters of dye samples with solvent pH.

pH	HOMO (*eV*)	LUMO (*eV*)	Band gap (*eV*)	LHE (%)
3,00	-4,77	-3,03	1,74	30,6
2,27	-4,76	-3,02	1,73	31,1
1,66	-4,74	-3,01	1,73	30,7
1,00	-5,21	-3,20	1,62	40,7

Table 4 and Fig. 8 summarise and illustrate the energy levels of each dye sample. As explained above, the pH of the solvent affects the chlorophyll content. In solvents with high pH, the chlorophyll content increases compared to solvents with lower pH. This results in a decrease in the energy band gap level due to the chlorophyll content.

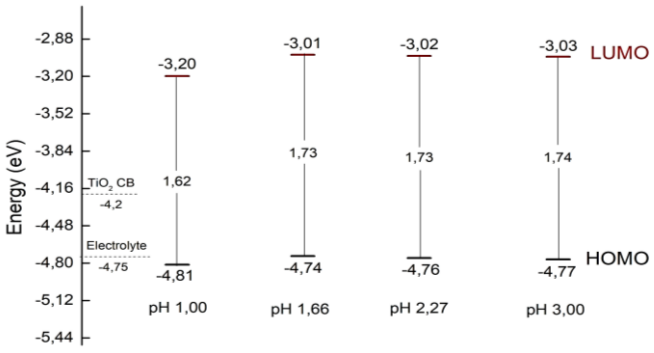

Fig. 8. Schematic diagram of dye energy levels with solvent pH.

This can occur because there is a difference in the amount or concentration of H^+ ions in the solvent. The more acidic, the number of H^+ ions will be greater so that it becomes a strong reason for the potential shift required for oxidation and reduction. Research conducted by Suyitno et al. [83] reported that changes from pH 4.00 to pH 3.00 resulted in changes in the band

gap value of papaya leaf extract energy from -2.2 eV to -2.15 eV.

The performance of DSSC was measured from the results of J-V characterization performed on all samples at sunlight intensity. From these measurements, the values of open circuit voltage (V_{OC}) and short circuit current density (J_{SC}) were obtained. In addition, conventional dye N179 was tested in the same way as a standard comparison. The values of V_{OC}, J_{SC}, fill factor and efficiency of each sample are shown in Table 4.

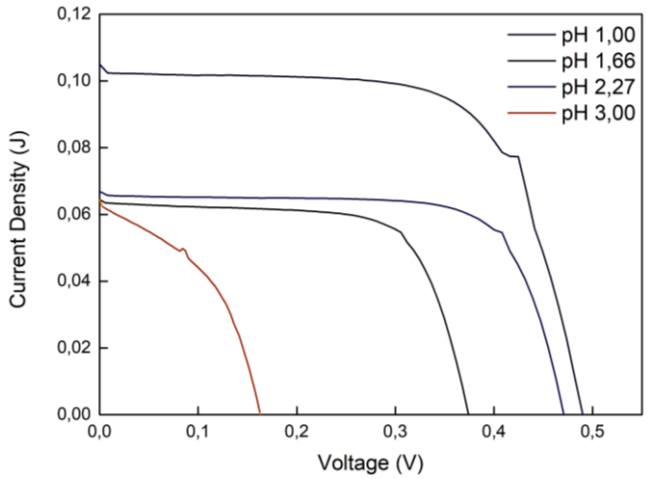

Fig. 9. J-V curves of DSSC samples with solvent pH.

Figures 9 and 10 show the current density graphs of each sample against voltage. Dye from Ageratum conyziodes leaves produced V_{OC} between 0.163 to 0.490 V, and J_{SC} values of 0.064 to 0.105 $\mu A/cm^2$. The dye sample with pH 1.00 solvent had the highest V_{OC} and J_{SC} compared to the other samples. However, the highest fill factor belongs to pH 2.27 with 71.5% and the smallest FF value is 43% which belongs to pH 3.00. The sample with the best efficiency was pH 1.00, where $\eta_{pH\ 1.00} > \eta_{pH\ 2.27} > \eta_{pH\ 1.66} > \eta_{pH\ 3.00}$. The effect of solvent pH on chlorophyll is significant; the more acidic the solvent, the better it is for chlorophyll [31]. However, there are many factors that make DSSC efficiency fluctuate, such as the compatibility of HOMO and LUMO energy levels that enable effective dye injection and regeneration processes, photoexcitation, and recombination processes [84]. Electron lifetime is one of the aspects considered because the greater number of molecules present due to the influence of solvent pH can cause electrons not to reach TiO_2 [85]

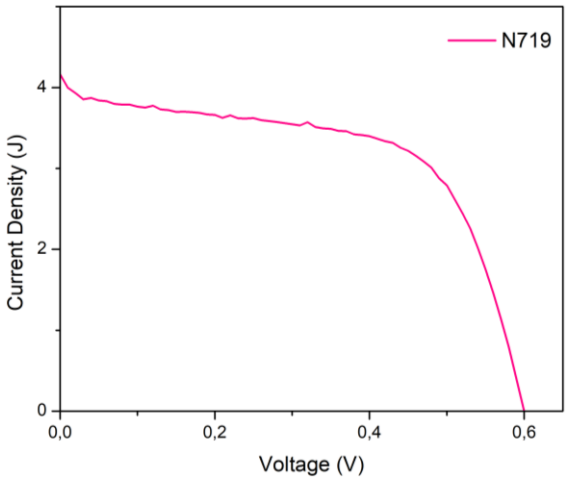

Fig. 10. J-V curve of DSSC sample with N719 dye.

Table 4. Photovoltaic parameters of DSSC samples with solvent pH.

pH	$V_{OC}(V)$	$J_{SC}(mA/cm^2)$	$FF(\%)$	$Eff(\times 10^{-4}\%)$
3,00	0,490	0,105	65,9	3,39
2,27	0,374	0,064	69,3	1,67
1,66	0,471	0,067	71,5	2,25
1,00	0,163	0,064	43	0,45

As a comparison, dye N719 was applied to the same DSSC component and produced an efficiency of 3.49%. The efficiency of the best efficiency sample made with pH 1.00 solvent was 0.000339% with the same component.

4.2. Effect of Dye Extractant Concentration on Photosensitizer Optical Properties and DSSC Performance

In previous research, using the pH of the solvent produces the best performance, namely pH 1.00. Research on the effect of the weight of dye-extracting leaf powder was carried out by varying the weight of A. Conyziodes powder, among others, is 1.25 grams, 3.75 grams, and 5 grams dissolved in 50 ml of solvent each. The absorbance test was conducted using UV-Vis Spectrometry, and an absorption graph of each weight of leaf powder was produced, as shown in Fig. 11.

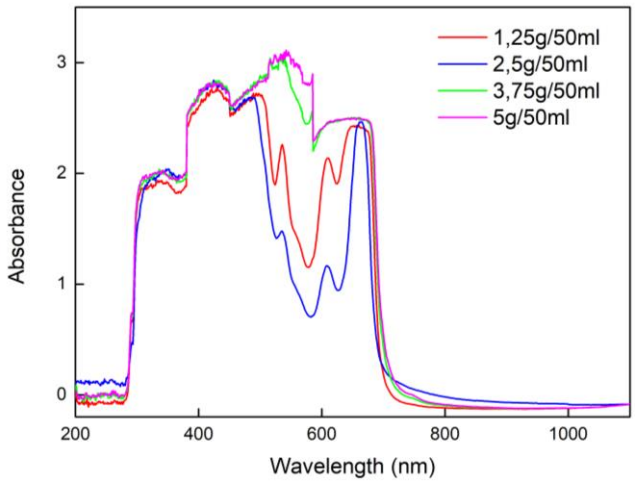

Fig. 11. UV-Vis absorption spectra of dye with Ageratum Conyziodes concentration against solvent.

The UV-Vis concentration graph is not much different in pattern from the UV-Vis pH solvent results. Chlorophyll A and cyanidin 3,5 diglucoside were still visible in each sample. However, the absorption intensity peaks were given by both phytoconstituents. Tables 6 and 7 show the effect of solvent concentration on the concentration of cyanidin 3.5 diglucoside, but not too much effect on the concentration of chlorophyll A.

Table 6. Effect of changing solvent concentration on chlorophyll A concentration.

Concentr-ation	λ Soret band chloroph-yll A (nm)	Chlorophyll A concentration (mM)	λ Q band chlorop-hyll A (nm)
1,25g/50ml	430	25,0	660
2,5g/50ml	424	25,4	661
3,75g/50ml	433	25,4	648
5g/50ml	425	25,3	660

Table 7. Effect of changing solvent concentration on Cyanidin 3,5-diglucoside concentration.

Concentration	λ Cyanidin 3,5 - diglucoside (nm)	Cyanidin 3,5 - diglucoside concentration (mM)
1,25g/50ml	430	25,0
2,5g/50ml	424	25,4
3,75g/50ml	433	25,4
5g/50ml	425	25,3

Increasing the solvent concentration increased the anthocyanin concentration, which can be seen in the concentrations 1.25g/50ml, 3.75g/50ml, and 5g/50ml. However, the increase did not have a significant effect on chlorophyll A. This large increase in cyanidin 3,5 diglucoside concentration made the anthocyanin absorption intensity peak the largest absorption peak in the 3.75g/50ml and 5g/50ml samples. The more significant number of dye molecules results in an increase in intensity [85]. In the 1.25g/50ml and 2.5g/50ml samples, the soret band belonging to chlorophyll A is still the absorption peak. In addition, there was an absorption shift in the 600-800 nm wavelength range. This shift occurred due to the increase in intensity as the weight of the leaf powder increased, which was caused by the increased concentration of cyanidin 3,5 diglucoside. Conradie [84] explains that the shift towards a larger wavelength (red shift) occurs due to changes in the dye molecule's electron structure, which enlarges the molecular mass.

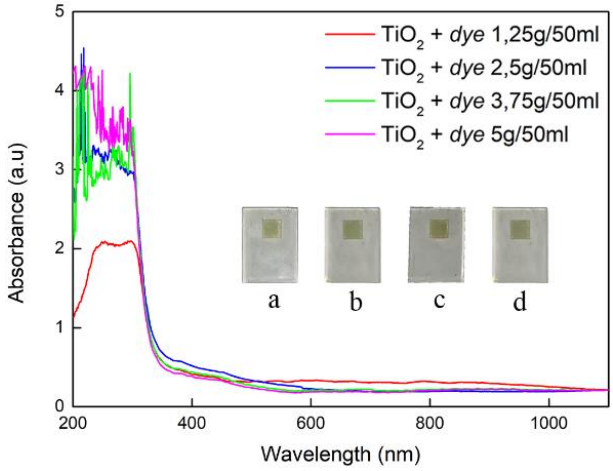

Fig. 12. UV-Vis Spectrometry graph of TiO_2 + Dye against the effect of solvent concentration.

The UV-Vis result graph of TiO_2 thin film that has been soaked for three days is shown in Fig. 12. The addition of dye can functionally increase the absorption range of TiO_2 in the visible and ultraviolet light range, just like the previous solvent pH results. However, the increase in concentration is not proportional to the increase in absorbance intensity in the 380-700 nm range. The graph shows that the 1.25g/50ml concentration has the highest intensity at wavelengths from 700 nm to 500 nm. In the other wavelength range (500-380 nm), the 2.5g/50ml concentration rose to overtake the absorbance intensity produced by the 1.25g/50ml concentration. The 3.75g/50ml and 5g/50ml concentrations had smaller intensities than the other samples. In both concentrations, the more leaf powder added, the lower the absorption in the visible light range. Meanwhile, in the ultraviolet range, the 2.5g/50ml concentration has the greatest overall intensity of 4.55 a.u at a wavelength of 218 nm. The order of absorbance peaks is $A_{Max\ 2.5g/50ml} > A_{Max\ 5g/50ml} > A_{Max\ 3.75g/50ml} > A_{Max\ 1.25g/50ml}$. This can occur because of the ability of TiO_2 to bind molecules, there is a limit and a maximum amount, so increasing the dye concentration does not always increase the ability to absorb light [86].

To find out the band gap value, a Tauck's Plot graph is made, as in Fig. 13, from the absorbance value of the dye. The results of this band gap analysis will then be

used as a reference again to determine HOMO and LUMO. The largest band gap value is owned by the concentration of 1.25g/50ml at 1.74 eV, and the smallest is owned by the concentration of 2.5g/50ml at 1.62 eV, as in Table 8. However, the band gap trend and the effect of changes in the concentration of cyanidin 3,5 diglucoside were examined. The increase in anthocyanin concentration narrows the band gap by weighing 2.5g/50ml, which is the same difference as the pH condition of the solvent.

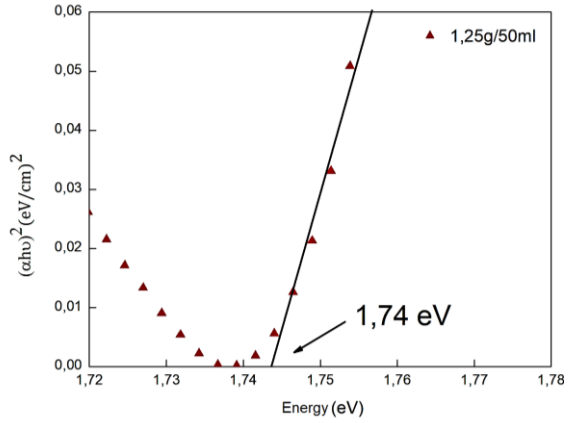

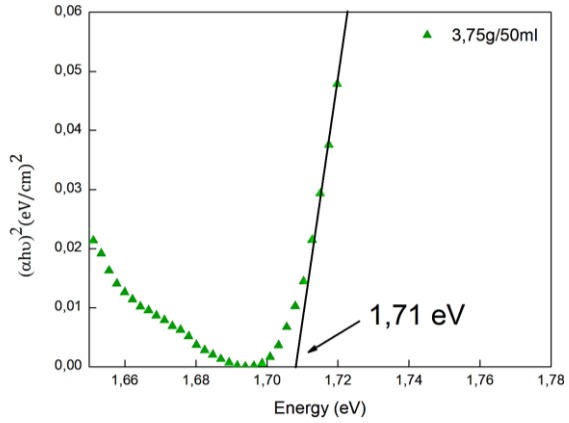

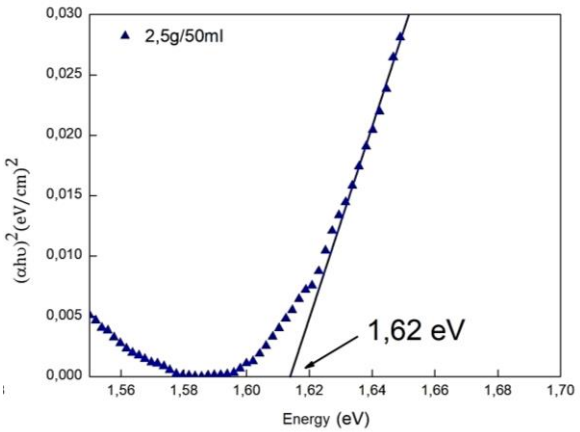

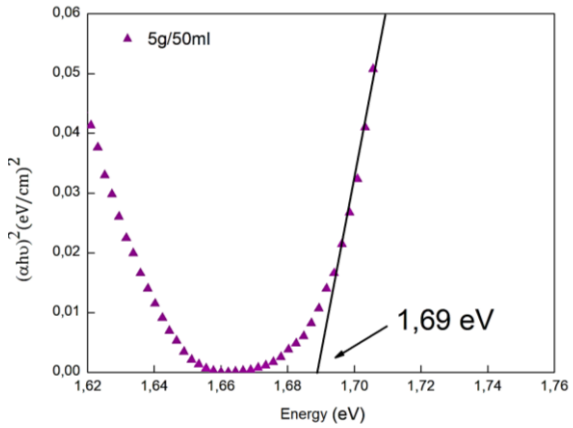

Fig. 13. Tauc's plot of dye samples with solvent concentration.

The graph in Fig. 14 shows the Light Harvesting Efficiency (LHE) percentage for each dye concentration sample. The change in solution concentration has an impact on the LHE peak percentage; the more leaves added to the solvent, the higher the resulting LHE peak. However, if the LHE percentage of each sample is averaged, the highest average LHE value is 40.7%, belonging to the 2.5g/50ml concentration, followed by the 5g/50ml concentration with 35.8%, and 3.75g/50ml with an average of 34.5%. Meanwhile, the lowest average LHE was found in the dye with a concentration of 1.25g/50ml, which was 30.3%.

While light-harvesting efficiency (LHE) is a critical factor for DSSC performance, it does not always correlate consistently with performance metrics like short-circuit current density (Jsc) or open-circuit voltage (Voc). Several factors could explain this discrepancy. High LHE indicates effective photon absorption by the dye, but this does not guarantee that all excited electrons are successfully injected into the TiO_2 conduction band. Recombination of excited electrons with oxidized dye molecules or the redox couple in the electrolyte can significantly reduce the photocurrent (Jsc) and overall efficiency, even when LHE is high.

A high concentration of dye molecules may enhance LHE but can lead to aggregation on the TiO_2 surface. Aggregates can hinder electron injection by disrupting molecular alignment and reducing the number of active sites for efficient electron transfer. This could explain why Jsc does not increase proportionally with LHE in some cases.

The alignment of the dye's HOMO and LUMO energy levels with the TiO_2 conduction band and the redox couple is crucial. Even with high LHE, inefficient energy level alignment can limit the electron injection rate or dye regeneration, reducing Voc and Jsc.

LHE measures the dye's ability to absorb light but does not account for how effectively this absorbed light is converted into electrical energy. Factors such as inefficient charge transfer at the electrode interfaces or poor electrolyte conductivity can diminish DSSC performance despite strong light absorption.

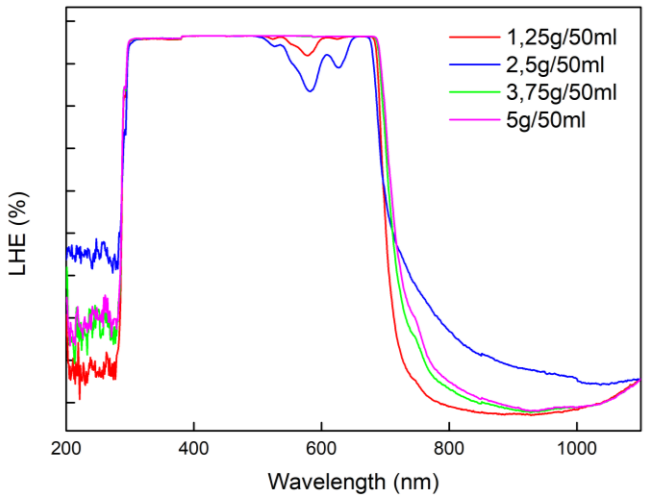

Fig. 14. Percentage of Light Harvesting Efficiency (LHE) of dye samples with solvent concentration.

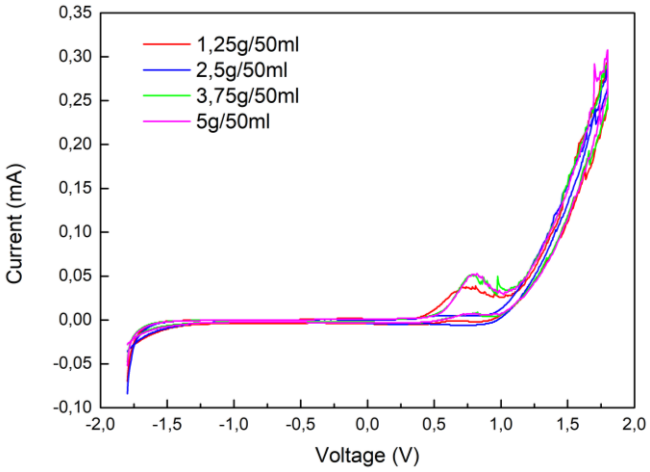

Fig. 15. Cyclic Voltammetry graph of dye sample with solvent concentration.

Photodegradation or thermal instability of the dye can reduce its ability to maintain efficient electron injection over time [87]. This instability may cause a decline in Voc and Jsc even if LHE remains initially high.

The lack of consistent correlation between LHE and DSSC performance metrics highlights the multifaceted nature of DSSC efficiency. Beyond light absorption, factors like electron recombination, dye aggregation, energy level alignment, and material stability all play significant roles. Addressing these issues through improved dye formulations, surface treatments, or optimized device architecture could enhance the alignment between LHE and performance metrics.

To determine the voltage at the time of dye oxidation, the Cyclic Voltammetry (CV) method is used. The results of the CV graph reading are shown in Fig. 15. The results of the analysis show that the oxidation energy (E_{oks}) tends to be similar, for concentrations of 1.25g/50ml, 2.5g/50ml, and 3.75g/50ml, the oxidation energy is 0.41 V, and for 5g/50ml, it is 0.42 V. This energy is then used to determine the HOMO energy level on the dye which is shown in Table 7.

Table 8 and Fig. 16 provide a summary and illustration of the energy levels for each dye sample. The LUMO calculation is the same as the previous solvent pH effect. Based on the highest LUMO value obtained by a concentration of 5g/50ml with a value of -3.12 eV and the lowest LUMO value obtained by a concentration of 2.5g/50ml with a value of -3.20 eV. Changes in concentration affect the decrease in LUMO level. Setiarso et al. [88] obtained similar results on the combination of anthocyanin and chlorophyll dyes from Curcuma xanthorrhiza and Anredera cordifolia extracts at pH 1.2 and pH 1.5 with leaf powder weights of 1:4 and 2:3 respectively, increasing anthocyanin concentration and stagnant chlorophyll concentration had an effect on decreasing the LUMO level.

Table 8. Electrochemical parameters of dye samples with solvent concentration.

Concentr-ation	HOMO (eV)	LUMO (eV)	Band gap (eV)	LHE (%)
1,25g/50ml	-4,81	-3,07	1,74	30,3
2,5g/50ml	-4,81	-3,20	1,62	40,7
3,75g/50ml	-4,81	-3,11	1,71	34,5
5g/50ml	-4,82	-3,12	1,69	35,8

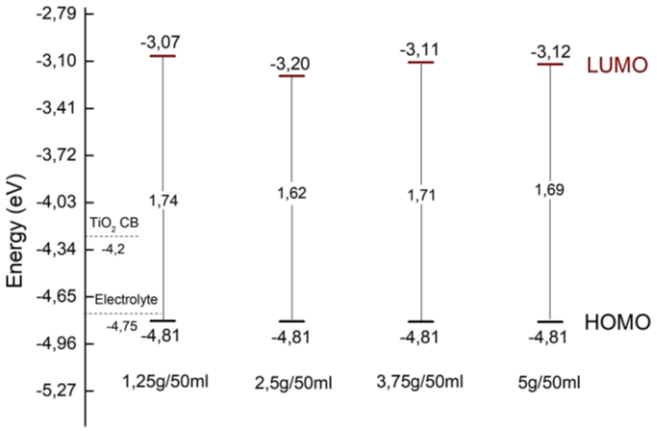

Fig. 16. Schematic diagram of dye energy levels with solvent concentration.

The performance of the DSSC was evaluated using the results of J-V characterization performed on all samples under sunlight intensity. From this measurement, the open circuit voltage (V_{OC}) and short circuit current (J_{SC}) values were obtained. Figure 17 shows the J-V graph curve. The values of V_{OC}, J_{SC}, fill factor and efficiency of each sample are shown in Table 9.

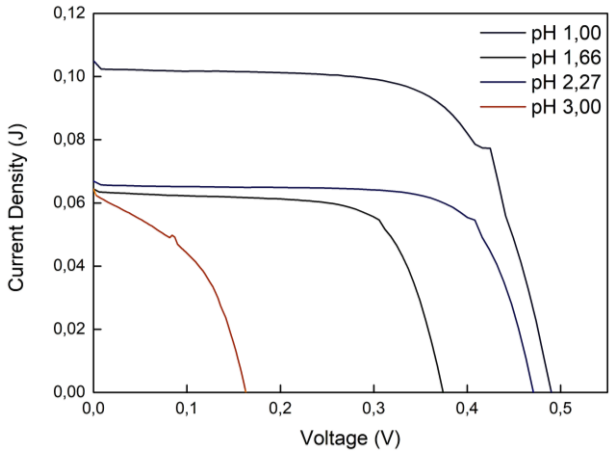

Fig. 17. J-V curves of DSSC samples with solvent pH.

The four samples have an average V_{OC} in the range of 0.337 V to 0.547 V, respectively. The average J_{SC} of the four samples was in the range $0{,}133 - 0{,}197\ mA/cm^2$. The largest $\overline{J_{SC}}$ value belongs to the sample with a concentration of 2.5g/50ml and the largest $\overline{V_{OC}}$ is shown by the sample with a concentration of 1.25g/50ml. The table shows the trend of $\overline{V_{OC}}$ decreasing as the solvent concentration increases. The largest average fill factor (FF) was shown by the concentration of 3.75g/50ml with a value of 64.1% and the order of $\overline{FF}$ from largest to smallest is $\overline{FF}_{3,75g/50ml} > \overline{FF}_{2,5g/50ml} > \overline{FF}_{5g/50ml} > \overline{FF}_{1,25g/50ml}$.

Table 9. Photovoltaic parameters of DSSC samples with solvent pH.

Concentration	$\overline{V_{OC}}(V)$	$\overline{J_{SC}}(mA/cm^2)$	$\overline{FF}$(%)	$\overline{Eff}.(\times 10^{-4}\%)$
1,25g/50ml	0,490	0,105	65,9	3,39
2,5g/50ml	0,374	0,064	69,3	1,67
3,75g/50ml	0,471	0,067	71,5	2,25
5g/50ml	0,163	0,064	43	0,45

The sample with the best average efficiency showed a concentration of 2.5g/50ml, where $\bar{\eta}_{2,5g/50ml} > \bar{\eta}_{3,75g/50ml} > \bar{\eta}_{1,25g/50ml} > \bar{\eta}_{5g/50ml}$. The change in concentration on efficiency if we look at the average efficiency of the concentration of 2.5g/50ml as a comparison, then when $\bar{\eta}_{1,25g/50ml}$ the number of molecules is not optimal. However, when the concentration is 3.75g/50ml, the number of dye molecules formed is certainly more than the previous weight of leaf powder. But an increase in concentration can be an obstacle for electrons to get to TiO_2. In the explanation of light absorption by the dye seen in the UV-Vis graph, there is an increase in intensity as the concentration increases, which indicates that the number of dye molecules is increasing. The number of molecules formed will produce more excited electrons [89]. However, the graph also shows a shift in absorption as the concentration increases, indicating an increase in molecular weight. Increasing dye concentration does increase the number of molecules formed, but this can also lead to negative effects such as increased electron recombination, which ultimately decreases the efficiency of the device [90]. This occurs due to self-aggregation, which causes many dye molecules to instead become inactive after attaching to the TiO_2 surface [91]. Another study reported the same thing on Hylocereus costaricensis peel with concentrations of 5g:20ml, 10g:20ml, 15g:20ml, 20g:20ml, 25g:20ml, and 30g:20ml resulting in an optimal concentration at a concentration of 20g:20ml [86].

Dye aggregation is a common issue in DSSCs when natural dyes are used. Aggregation can occur when dye molecules cluster together on the TiO_2 surface instead of spreading evenly. This clustering reduces the surface area available for light absorption and limits the efficiency of electron injection into the TiO_2 conduction band. Evidence from UV-Vis spectroscopy in this study suggests that increased dye concentration may contribute to aggregation, as higher concentrations led to a red shift in absorption peaks, indicating molecular interactions that promote aggregation.

The functional groups identified in FTIR analysis, such as hydroxyl (-OH) and carbonyl (>C=O), are essential for anchoring dye molecules to the TiO_2 surface. However, if the dye molecules are not properly adsorbed or if the binding is weak, the electron transfer from the excited dye molecules to the TiO_2 conduction band may be inefficient. Variations in pH and extraction conditions could further impact the molecular binding process, as acidic environments can alter the dye's molecular structure and binding capacity.

Electron recombination occurs when excited electrons in the TiO_2 conduction band recombine with oxidized dye molecules or the redox couple in the electrolyte before reaching the external circuit. This significantly reduces the photocurrent and overall efficiency. The relatively low open-circuit voltage (Voc) and short-circuit current density (Jsc) observed in this study may indicate high rates of recombination. This issue could be exacerbated by suboptimal alignment of the dye's HOMO and LUMO levels with the TiO_2 conduction band and the redox couple, as shown in the cyclic voltammetry results.

Although the UV-Vis results demonstrated strong absorbance in specific regions (435–664 nm), the absorbance spectrum may not be broad enough to fully utilize the solar spectrum. Natural dyes, including those from Ageratum conyzoides L., typically lack the extended light absorption range of synthetic dyes like N719, which limits their overall light-harvesting efficiency (LHE).

Other factors, such as uneven coating of the dye on the TiO_2 film, suboptimal electrolyte composition, or insufficient light-harvesting due to dye degradation, could also contribute to the low efficiency. The maceration and extraction methods, while effective for maximizing pigment yield, might require further refinement to enhance dye stability and reduce degradation.

Recent studies have reported significant progress in improving the efficiencies of DSSCs using natural dyes. For instance, DSSCs using anthocyanin extracted from Malva verticillata and Syzygium cumini achieved an efficiency of 1.84% [19], while red cabbage-derived anthocyanins yielded an efficiency of 2.90% [9]. Additionally, a mixture of chlorophyll and anthocyanins from Hylocereus costaricensis achieved efficiencies exceeding 3.53% [25]. These studies attribute their improved efficiencies to the careful optimization of dye extraction processes, solvent selection, and molecular tailoring to enhance electron injection and light absorption.

In comparison, the efficiency reported in this study (0.000598%) is notably lower. This divergence is primarily due to the experimental focus on solvent pH and concentration, which, while foundational to understanding the dye's optical properties, did not yet optimize other critical factors such as dye aggregation, molecular stability, or electron recombination suppression. Furthermore, the use of Ageratum conyzoides L., a relatively underexplored natural dye source, introduces new insights into how specific phytochemicals, such as flavonoids and chlorophyll, perform under varied extraction conditions.

Unlike prior studies that primarily target maximizing efficiency, this work explores the fundamental effects of solvent pH and dye concentration, providing a detailed understanding of the molecular interactions influencing DSSC performance. This foundational approach lays the groundwork for future studies that can integrate these findings with additional optimizations—such as co-sensitization, surface treatment, or the use of alternative electrolytes—to achieve higher efficiencies. Thus, this study extends existing literature by introducing a novel dye source and systematically examining key parameters, while simultaneously diverging by focusing on scientific mechanisms rather than efficiency optimization alone.

5. Summary

Changes in solvent pH affect optical properties through changes in absorption intensity and chlorophyll and cyanidin concentrations. Increasing acidity increases chlorophyll concentration and decreases band gap energy, while cyanidin concentration decreases, indicating that low pH inhibits anthocyanin formation.

The values of V_{OC}, J_{SC}Fill factor and efficiency are parameters that determine the optimal DSSC performance. Tests on the performance of DSSCs with pH 1.00 solvent provide optimal performance compared to other pHs. The photovoltaic parameters obtained were V_{OC} of 0.490 V, J_{SC} of 0.105 mA/cm^2, fill factor of 65.9%, and efficiency of 0.000339%.

Meanwhile, the change in concentration affects the LUMO value, increases the anthocyanin concentration, and makes anthocyanin absorption more dominant. This causes a shift in wavelength absorption and a change in the dye's molecular structure, showing the significant impact of concentration on optical properties.

In addition, the best performance of DSSC is at a concentration of 2.5g/50ml against the solvent volume. The sample produced a value of $(\overline{V_{OC}})$ 0.525V, $(\overline{J_{SC}})$ 0.197 mA/cm^2 , fill factor 58.4%, and efficiency 0.000598%. The decrease in performance after the optimum concentration is due to the aggregation of dye molecules, which reduces the effectiveness of electron transfer.

Acknowledgment

This research was funded by the Ministry of Higher Education, Science, and Technology; and Universitas Pendidikan Indonesia 2025 through a research grant awarded to the Solar Energy Materials research group of Universitas Pendidikan Indonesia.

References

[1] U. Mahajan, K. Prajapat, M. Dhonde, K. Sahu, and P. M. Shirage, "Natural dyes for dye-sensitized solar cells (DSSCs): An overview of extraction, characterization and performance," *Nano-Structures & Nano-Objects*, vol. 37, p. 101111, 2024. [Online]. Available: https://doi.org/10.1016/j.nanoso.2024.101111

[2] A. Błaszczyk, K. Joachimiak-Lechman, S. Sady, T. Tański, M. Szindler, and A. Drygała, "Environmental performance of dye-sensitized solar cells based on natural dyes," *Solar Energy*, vol. 215, pp. 346–355, 2021. [Online]. Available: https://doi.org/10.1016/j.solener.2020.12.040

[3] P. Prakash and B. Janarthanan, "Review on the progress of light harvesting natural pigments as DSSC sensitizers with high potency," *Inorganic Chemistry Communications*, vol. 152, p. 110638, 2023. [Online]. Available: https://doi.org/10.1016/j.inoche.2023.110638

[4] S. Çakar, M. Özacar, and F. Fındık, "MOFs-based dye-sensitized photovoltaics," in *Micro and Nano Technologies*, R. K. Gupta, T. A. Nguyen, and G. B. T.-M.-O. F.-B. N. for E. C. and S. Yasin, Eds. Elsevier, 2022, ch. 22, pp. 487–506. [Online]. Available: https://doi.org/10.1016/B978-0-323-91179-5.00033-4

[5] B. O'Regan and M. Grätzel, "A low-cost, high-efficiency solar cell based on dye-sensitized colloidal TiO_2 films," Nature, vol. 353, no. 6346, pp. 737–740, 1991. [Online]. Available: https://doi.org/10.1038/353737a0

[6] H. Peng, X. Sun, W. Weng, and X. Fang, "Energy harvesting based on polymer," in *Polymer Materials for Electronics and Energy Applications*, H. Peng, X. Sun, W. Weng, and X. Fang, Eds. Academic Press, 2017, pp. 151–196. [Online]. Available:

https://doi.org/10.1016/B978-0-12-811091-1.00005-7

[7] K. Sharma, V. Sharma, and S. S. Sharma, "Dye-sensitized solar cells: Fundamentals and current status," *Nanoscale Research Letters*, vol. 13, 2018. [Online]. Available: https://doi.org/10.1186/s11671-018-2760-6

[8] S. Singh, I. C. Maurya, S. Sharma, S. P. S. Kushwaha, P. Srivastava, and L. Bahadur, "Application of new natural dyes extracted from Nasturtium flowers (Tropaeolum majus) as photosensitizer in dye-sensitized solar cells," *Optik*, vol. 243, p. 167331, 2021. [Online]. Available: https://doi.org/10.1016/j.ijleo.2021.167331

[9] G. Calogero, A. Bartolotta, G. Di Marco, A. Di Carlo, and F. Bonaccorso, "Vegetable-based dye-sensitized solar cells," *Chemical Society Reviews*, vol. 44, no. 10, pp. 3244–3294, 2015. [Online]. Available: https://doi.org/10.1039/C4CS00309H

[10] G. Calogero *et al.*, "Absorption spectra, thermal analysis, photoelectrochemical characterization and stability test of vegetable-based dye-sensitized solar cells," *Optical Materials*, vol. 88, pp. 24–29, 2019. [Online]. Available: https://doi.org/10.1016/j.optmat.2018.11.005

[11] J. Wu, Z. Lan, J. Lin, M. Huang, Y. Huang, L. Fan, G. Luo, Y. Lin, Y. Xie, and Y. Wei, "Counter electrodes in dye-sensitized solar cells," *Chemical Society Reviews*, vol. 46, no. 19, pp. 5975–6023, 2017. [Online]. Available: https://doi.org/10.1039/c6cs00752j

[12] M. Bhogaita, A. D. Shukla, and R. P. Nalini, "Recent advances in hybrid solar cells based on natural dye extracts from Indian plant pigment as sensitizers," *Solar Energy*, vol. 137, pp. 212–224, 2016. [Online]. Available: https://doi.org/10.1016/j.solener.2016.08.003

[13] [13] M. Erdogdu, A. Atilgan, Y. Erdogdu, and A. Yildiz, "Flavonoid from *Hedera helix* fruits: A promising new natural sensitizer for DSSCs," *Journal of Photochemistry and Photobiology A: Chemistry*, vol. 448, p. 115288, 2024. [Online]. Available: https://doi.org/10.1016/j.jphotochem.2023.115288

[14] S. Borbón, S. Lugo, D. Pourjafari, N. Pineda Aguilar, G. Oskam, and I. López, "Open-circuit voltage (VOC) enhancement in TiO_2-based DSSC: Incorporation of ZnO nanoflowers and Au nanoparticles," *ACS Omega*, vol. 5, no. 19, pp. 10977–10986, 2020. [Online]. Available: https://doi.org/10.1021/acsomega.0c00794

[15] J. Nelson and R. E. Chandler, "Random walk models of charge transfer and transport in dye sensitized systems," *Coordination Chemistry Reviews*, vol. 248, no. 13, pp. 1181–1194, 2004. [Online]. Available: https://doi.org/10.1016/j.ccr.2004.04.001

[16] R. Nakhaei, A. Razeghizadeh, P. Shabani, J. Ganji, and S. S. Tabatabaee, "Combination of co-sensitization and Förster resonance energy transfer in natural-synthetic dye sensitized solar cells," *Optical Materials*, vol. 131, p. 112690, 2022. [Online]. Available: https://doi.org/10.1016/j.optmat.2022.112690

[17] P. S. Saud, A. Bist, A. A. Kim, A. Yousef, A. Abutaleb, M. Park, S. J. Park, and B. Pant, "Dye-sensitized solar cells: Fundamentals, recent progress, and optoelectrical properties improvement strategies," *Optical Materials*, vol. 150, p. 115242, Mar. 2024. [Online]. Available: https://doi.org/10.1016/j.optmat.2024.115242

[18] M. Yahya, A. Bouziani, C. Ocak, Z. Seferoğlu, and M. Sillanpää, "Organic/metal-organic photosensitizers for dye-sensitized solar cells (DSSC): Recent developments, new trends, and future perceptions," *Dyes and Pigments*, vol. 192, p. 109227, 2021. [Online]. Available: https://doi.org/10.1016/j.dyepig.2021.109227

[19] M. Golshan, S. Osfouri, R. Azin, T. Jalali, and N. R. Moheimani, "Co-sensitization of natural and low-cost dyes for efficient panchromatic light-harvesting using dye-sensitized solar cells," *Journal of Photochemistry and Photobiology A: Chemistry*, vol. 417, p. 113345, 2021. [Online]. Available: https://doi.org/10.1016/j.jphotochem.2021.113345

[20] G. Calogero and G. Di Marco, "Red Sicilian orange and purple eggplant fruits as natural sensitizers for dye-sensitized solar cells," *Solar Energy Materials and Solar Cells*, vol. 92, no. 11, pp. 1341–1346, 2008. [Online]. Available: https://doi.org/10.1016/j.solmat.2008.05.007

[21] A. S. Teja, A. Srivastava, J. A. K. Satrughna, M. K. Tiwari, A. Kanwade, S. Chand Yadav, and P. M. Shirage, "Optimal processing methodology for futuristic natural dye-sensitized solar cells and novel applications," *Dyes and Pigments*, vol. 210, Sept. 2022. [Online]. Available: https://doi.org/10.1016/j.dyepig.2022.110997

[22] G. Richhariya, A. Kumar, P. Tekasakul, and B. Gupta, "Natural dyes for dye sensitized solar cell: A review," *Renewable and Sustainable Energy Reviews*, vol. 69, pp. 705–718, Apr. 2015. [Online]. Available: https://doi.org/10.1016/j.rser.2016.11.198

[23] A. Bist and S. Chatterjee, "Review on efficiency enhancement using natural extract mediated dye-sensitized solar cell for sustainable photovoltaics," *Energy Technology*, vol. 9, no. 8, pp. 1–19, 2021. [Online]. Available: https://doi.org/10.1002/ente.202001058

[24] M. Z. Iqbal, S. R. Ali, and S. Khan, "Progress in dye sensitized solar cell by incorporating natural photosensitizers," *Solar Energy*, vol. 181, pp. 490–509, 2019. [Online]. Available: https://doi.org/10.1016/j.solener.2019.02.023

[25] V. Yadav, C. M. S. Negi, D. K. Kumar, and S. K. Gupta, "Fabrication of eco-friendly, low-cost dye sensitized solar cells using harda fruit-based natural

dye," *Optical Materials*, vol. 122, p. 111800, 2021. [Online]. Available: https://doi.org/10.1016/j.optmat.2021.111800

[26] A. Retnowati, R. Rugayah, J. S. Rahajoe, and D. Arifiani, *Status Keanekaragaman Hayati Indonesia: Kekayaan Jenis Tumbuhan dan Jamur Indonesia*, LIPI Press, Lembaga Ilmu Pengetahuan Indonesia, 2019. [Online]. Available: https://penerbit.brin.go.id/press/catalog/book/penerbit.brin.go.id/press/catalog/book/206

[27] S. K. Harefa, U. Zega, and A. S. Bago, "Pemanfaatan Daun Bandotan (*Ageratum conyzoides* L.) Sebagai Obat Tradisional Di Desa Bawoza'ua Kecamatan Telukdalam Kabupaten Nias Selatan," *Jurnal Pendidikan Biologi*, vol. 3, no. 1, pp. 14–24, 2022. [Online]. Available: https://jurnal.uniraya.ac.id/index.php/Tunas/article/view/477

[28] R. Hilaliyah, "Pemanfaatan Tumbuhan Liar Bandotan (*Ageratum conyzoides* L.) sebagai Obat Tradisional dan Aktivitas Farmakologinya," *Bioscientiae*, vol. 18, no. 1, p. 28, 2021. [Online]. Available: https://doi.org/10.20527/b.v18i1.4065

[29] N. Yadav, S. A. Ganie, B. Singh, A. K. Chhillar, and S. S. Yadav, "Phytochemical constituents and ethnopharmacological properties of Ageratum conyzoides L.," *Phytotherapy Research*, vol. 33, no. 9, pp. 2163–2178, 2019. [Online]. Available: https://doi.org/10.1002/ptr.6405

[30] A. Nasyori and F. A. Noor, "The effects of the concentration of red and yellow gambier fruit dyes on the short-circuit photocurrent in dye-sensitised solar cells," *Journal of Physics: Conference Series*, 2021. [Online]. Available: https://doi.org/10.1088/1742-6596/1811/1/012067

[31] A. K. Arof and T. L. Ping, "Chlorophyll as photosensitizer in dye-sensitized solar," in Chlorophyll, InTech, 2017, p. 105. [Online]. Available: https://doi.org/10.5772/67955

[32] N. T. R. N. Kumara, A. Lim, C. M. Lim, M. I. Petra, and P. Ekanayake, "Recent progress and utilization of natural pigments in dye sensitized solar cells: A review," *Renewable and Sustainable Energy Reviews*, vol. 78, pp. 301–317, 2017. [Online]. Available: https://doi.org/10.1016/j.rser.2017.04.075

[33] E. C. Cahya Prima, B. Yuliarto, S. Suyatman, and H. K. Dipojono, "Theoretical investigation of anthocyanidin aglycones as photosensitizers for dye-sensitized TiO_2 solar cells," *Advanced Materials Research*, vol. 1112, pp. 317–320, 2015. [Online]. Available: https://doi.org/10.4028/www.scientific.net/AMR.1112.317

[34] M. Al Qibtiya, E. C. Prima, B. Yuliarto, and S. Suyatman, "pH influences on optical absorption of anthocyanin from black rice as sensitizer for dye sensitized solar cell TiO_2 nanoparticles," *Materials Science Forum*, vol. 864, pp. 154–158, 2016. [Online]. Available: https://doi.org/10.4028/www.scientific.net/MSF.864.154

[35] N. J. Cherepy, G. P. Smestad, M. Grätzel, and J. Z. Zhang, "Ultrafast electron injection: Implications for a photoelectrochemical cell utilizing an anthocyanin dye-sensitized TiO_2 nanocrystalline electrode," *The Journal of Physical Chemistry B*, vol. 101, no. 45, pp. 9342–9351, 1997. [Online]. Available: https://doi.org/10.1021/jp972197w

[36] A. Munim, "Isolasi Dan Elusidasi Struktur Senyawa Flavonoida Dari *Crotalaria Anagyroides*," *Pharmaceutical Sciences and Research*, vol. 2, no. 1, pp. 22–29, 2005. [Online]. Available: https://doi.org/10.7454/psr.v2i1.3381

[37] M. Z. Najihah, I. M. Noor, and T. Winie, "Long-run performance of dye-sensitized solar cell using natural dye extracted from Costus woodsonii leaves," *Optical Materials*, vol. 123, p. 111915, 2022. [Online]. Available: https://doi.org/10.1016/j.optmat.2021.111915

[38] N. Hindryawati, I. A. Hiyahara, H. Saputra, M. S. Arief, and G. P. Maniam, "Preparation of dye-sensitized solar cell (DSSC) using TiO_2 and Mahkota Dewa fruit (*Phaleria macrocarpa* (Scheff) Boerl.) extract," *Jurnal Bahan Alam Terbarukan*, vol. 10, no. 1, pp. 43–49, 2021. [Online]. Available: https://doi.org/10.15294/jbat.v10i1.32378

[39] E. C. Prima, P. F. Rusliani, E. Suhendi, and B. Yuliarto, "Performance of dye-sensitized solar cells with mixed three natural pigments and reduced graphene oxide as a counter electrode," *Results in Optics*, vol. 14, p. 100592, 2024. [Online]. Available: https://doi.org/10.1016/j.rio.2023.100592

[40] A. Supriyanto, C. Cari, S. Khairuddin, P. M. Suciatmoko, D. Kurniawan, and T. Y. Septiawan, "The fabrication of DSSC TiO2 transparent thin layer with natural dye sweet potato (Ipomoea batatas L.)," *Journal of Physics: Conference Series*, vol. 1153, no. 1, pp. 8–12, 2019. [Online]. Available: https://doi.org/10.1088/1742-6596/1153/1/012098

[41] D. Martineau, *Dye Solar Cells for Real The Assembly Guide for Making Your Own Solar Cells*. Solaronix SA, 2012. [Online]. Available: https://www.solaronix.com/

[42] P. Cheng, L. Yang, Y. Liu, J. Liu, and Y. Fan, "Promotion of sugar extraction from sewage sludge by microwave combined with thermal-alkaline pretreatment," *Water (Switzerland)*, vol. 15, no. 7, 2023. [Online]. Available: https://doi.org/10.3390/w15071291

[43] I. Greco, C. Varon, and C. S. Iorio, "Synthesis and characterization of a new alginate-gelatine aerogel for tissue engineering," in *Proc. Annu. Int. Conf. IEEE Eng. Med. Biol. Soc. (EMBS)*, Jul. 2022, pp. 3915–3918. [Online]. Available: https://doi.org/10.1109/EMBC48229.2022.9871508

[44] P. A. Sieck, K. Hukari, J. Countrywood, and V. Kodash, "Stoichiometry of DC sputtered WO3," *Solar and Switching Materials*, vol. 4458, pp. 219–225, Nov. 2001. [Online]. Available: https://doi.org/10.1117/12.448259

[45] S. Sobhanardakani, A. Jafari, R. Zandipak, and A. Meidanchi, "Removal of heavy metal (Hg(II) and Cr(VI)) ions from aqueous solutions using Fe2O3@SiO2 thin films as a novel adsorbent," *Process Safety and Environmental Protection*, vol. 120, pp. 348–357, Nov. 2020. [Online]. Available: https://doi.org/10.1016/j.psep.2018.10.002

[46] B. D. Assresahegn and D. Bélanger, "Synthesis of binder-like molecules covalently linked to silicon nanoparticles and application as anode material for lithium-ion batteries without the use of electrolyte additives," *Journal of Power Sources*, vol. 345, pp. 190–201, 2017. [Online]. Available: https://doi.org/10.1016/j.jpowsour.2017.01.135

[47] F. C. Bombaldi De Souza, R. F. Bombaldi De Souza, and A. M. Moraes, "Incorporation and release kinetics of alpha-bisabolol from PCL and chitosan/guar gum membranes," *Brazilian Journal of Chemical Engineering*, vol. 33, no. 3, pp. 453–467, 2016. [Online]. Available: https://doi.org/10.1590/0104-6632.20160333s20150083

[48] F. Ferati, "Structural information from ratio bands in the FTIR spectra of long chain and branched alkanes in petrodiesel samples," *Journal of Environmental Treatment Techniques*, vol. 8, no. 3, pp. 1140–1143, 2020.

[49] M. Khyade, S. P. Sanstha, and S. N. Arts, "Chemical profiling and free radical scavenging potential of *Oxalis corniculata*," *Explorer*, vol. 1, no. 1, pp. 88–93, 2016.

[50] S. N. A. Kumar, S. K. Ritesh, G. Sharmila, and C. Muthukumaran, "Extraction optimization and characterization of water soluble red purple pigment from floral bracts of *Bougainvillea glabra*," *Arabian Journal of Chemistry*, vol. 10, pp. S2145–S2150, 2017. [Online]. Available: https://doi.org/10.1016/j.arabjc.2013.07.047

[51] W. Lao, G. Li, Q. Zhou, and T. Qin, "Quantitative analysis of biomass in three types of wood-plastic composites by FTIR spectroscopy," *BioResources*, vol. 9, no. 4, pp. 6073–6086, 2014. [Online]. Available: https://doi.org/10.15376/biores.9.4.6073-6086

[52] M. Namie, J.-H. Kim, and S. Yonezawa, "Enhanced dyeing of polypropylene using fluorine–oxygen gas mixtures," *Colorants*, vol. 2, no. 3, pp. 552–564, 2023. [Online]. Available: https://doi.org/10.3390/colorants2030027

[53] S. R. Yenumala, S. K. Maity, and D. Shee, "Hydrodeoxygenation of Karanja Oil over Supported Nickel Catalysts: Roles of support and nickel loading on yAl2O3," *4*, no. 1, pp. 1–6, 2015.

[54] T. Endo *et al.*, "Composite engineering – Direct bonding of plastic PET films by plasma irradiation," *Procedia Engineering*, vol. 171, pp. 88–103, 2017. [Online]. Available: https://doi.org/10.1016/j.proeng.2017.01.315

[55] Y. Guo and P. Wu, "FTIR spectroscopic study of the acrylamide states in AOT reversed micelles," *Journal of Molecular Structure*, vol. 883–884, no. 1–3, pp. 31–37, 2008. [Online]. Available: https://doi.org/10.1016/j.molstruc.2007.11.009

[56] Y. Hirashima, H. Sato, Y. Miyashita, and A. Suzuki, "ATR-FTIR spectroscopic study on hydrogen bonding of polyelectrolyte hydrogels," *Polymer Preprints, Japan*, vol. 54, no. 1, p. 1270, 2005.

[57] M. Alauhdin, W. T. Eden, and D. Alighiri, "Aplikasi spektroskopi inframerah untuk analisis tanaman dan obat herbal," *Inovasi Sains dan Kesehatan*, pp. 84–118, 2021. [Online]. Available: https://doi.org/10.15294/.v0i0.15

[58] P. Calvini and A. Gorassini, "FTIR - Deconvolution spectra of paper documents," *Restaurator*, vol. 23, no. 1, pp. 48–66, 2002. [Online]. Available: https://doi.org/10.1515/REST.2002.48

[59] G. Dedeepya *et al.*, "Dyes prepared from leaf extract of siriyanangai (*Andrographis paniculata*) with the effect of TiO_2 based DSSCs," *Materials Today: Proceedings*, vol. 66, pp. 3644–3650, 2022. [Online]. Available: https://doi.org/10.1016/j.matpr.2022.07.188

[60] S. Lefrant, M. Baibarac, and I. Baltog, "Raman and FTIR spectroscopy as valuable tools for the characterization of polymer and carbon nanotube based composites," *Journal of Materials Chemistry*, vol. 19, no. 32, pp. 5690–5704, 2009. [Online]. Available: https://doi.org/10.1039/b821136a

[61] *Nature*, "Conjugated aromatic systems," *Nature Synthesis*, vol. 2, no. 9, p. 799, 2023. [Online]. Available: https://doi.org/10.1038/s44160-023-00404-5

[62] J. Poater, M. Duran, M. Solà, and B. Silvi, "Theoretical evaluation of electron delocalization in aromatic molecules by means of atoms in molecules (AIM) and electron localization function (ELF) topological approaches," *Chemical Reviews*, vol. 105, no. 10, pp. 3911–3947, 2005. [Online]. Available: https://doi.org/10.1021/cr030085x

[63] E. K. Elmaghraby, S. Abdelaal, A. M. Abdelhady, S. Fares, S. Salama, and N. A. Mansour, "Correspondence and difference between gamma-ray and neutron irradiation effects on organic materials in marine environment," *Egyptian Journal of Aquatic Biology and Fisheries*, vol. 23, no. 5 Special Issue, pp. 1–16, 2019. [Online]. Available: https://doi.org/10.21608/ejabf.2019.63408

[64] I. M. Ibrahim, S. Yunus, and M. A. Hashim, "Relative performance of isopropylamine, pyrrole and pyridine as corrosion inhibitors for carbon steels in saline water at mildly elevated temperatures," *International Journal of Scientific & Engineering Research*, vol. 4, no. 2, pp. 1–12, 2013.

[65] S. Mutingatun, E. Fachriyah, and D. Kusrini, "Isolation, identification, and antioxidant activity of flavonoid compounds in the ethanol extract in Bandotan leaves (Ageratum conyzoides)," *Jurnal Kimia Sains dan Aplikasi*, vol. 25, no. 12, pp. 456–466, 2022. [Online]. Available: https://ejournal.undip.ac.id/index.php/ksa/article/view/53056

[66] S. Pangajavalli, R. Ranjithkumar, B. Sridhar, and S. Ramaswamy, "Hirshfeld and vibrational analysis of 5-Benzyl-7a-Hydroxy-1-Methyl-2,3,5,6,7,7a-Hexahydro-1H-3a, 7-Methanoindeno [2,1-d]Pyrrolo[3,2-c]Azepine-12,13(4H)-Dione," *Mechanics, Materials Science & Engineering Journal*, 2017.

[67] L. Rastogi and J. Arunachalam, "Sunlight based irradiation strategy for rapid green synthesis of highly stable silver nanoparticles using aqueous garlic (Allium sativum) extract and their antibacterial potential," *Materials Chemistry and Physics*, vol. 129, no. 1–2, pp. 558–563, 2011. [Online]. Available: https://doi.org/10.1016/j.matchemphys.2011.04.068

[68] S. A. Kustrin, V. Gegechkori, D. S. Petrovich, K. T. Ilinichna, and D. W. Morton, "ATR-FTIR characterisation of major flavonoids and polyphenolics," *Molecules*, vol. 26, p. 6892, 2021.

[69] A. P. Kusumadewi, R. Martien, S. Pramono, A. A. Setyawan, A. Windarsih, and A. Rohman, "Application of FTIR spectroscopy and chemometrics for correlation of antioxidant activities, phenolics and flavonoid contents of Indonesian *Curcuma xanthorrhiza*," *International Journal of Food Properties*, vol. 25, no. 1, pp. 2364–2372, 2022. [Online]. Available: https://doi.org/10.1080/10942912.2022.2134418

[70] R. N. Oliveira, M. C. Mancini, F. C. S. de Oliveira, T. M. Passos, B. Quilty, R. M. da S. M. Thiré, and G. B. McGuinness, "Análise por FTIR e quantificação de fenóis e flavonóides de cinco produtos naturais disponíveis comercialmente utilizados no tratamento de feridas," *Revista Materia*, vol. 21, no. 3, pp. 767–779, 2016. [Online]. Available: https://doi.org/10.1590/S1517-707620160003.0072

[71] S. Thummajitsakul and K. Silprasit, "Analysis of FTIR Spectra, Flavonoid Content and Anti-Tyrosinase Activity of Extracts and Lotion from Garcinia schomburgkiana by Multivariate Method," *Trends in Sciences*, vol. 19, no. 18, 2022. [Online]. Available: https://doi.org/10.48048/tis.2022.5780

[72] N. Bhattacharjee and A. B. Biswas, "Pyrolysis of *Ageratum conyzoides* (goat weed): Parametric influence on the product yield and product characterization," *Journal of Thermal Analysis and Calorimetry*, vol. 139, no. 2, pp. 1515–1536, 2020. [Online]. Available: https://doi.org/10.1007/s10973-019-08437-9

[73] A. B. D. Nandiyanto, R. Oktiani, and R. Ragadhita, "How to read and interpret FTIR spectroscope of organic material," *Indonesian Journal of Science and Technology*, vol. 4, no. 1, pp. 97–118, 2019. [Online]. Available: https://doi.org/10.17509/ijost.v4i1.15806

[74] Y. Koyama, Y. Umemoto, A. Akamatsu, K. Uehara, and M. Tanaka, "Raman spectra of chlorophyll forms," *Journal of Molecular Structure*, vol. 146, no. C, pp. 273–287, 1986. [Online]. Available: https://doi.org/10.1016/0022-2860(86)80299-X

[75] S. Sravan Kumar, P. Manoj, and P. Giridhar, "Fourier transform infrared spectroscopy (FTIR) analysis, chlorophyll content and antioxidant properties of native and defatted foliage of green leafy vegetables," *Journal of Food Science and Technology*, vol. 52, no. 12, pp. 8131–8139, 2015. [Online]. Available: https://doi.org/10.1007/s13197-015-1959-0

[76] C. Nurfaizah, D. Krisdiyanto, K. Khamidinal, and S. Sudarlin, "Krokot extract (Portulaca oleracea. L) as natural light-harvesting pigments for dye-sensitized solar cells (DSSCs): Influence of dye acidity," *Biology, Medicine, & Natural Product Chemistry*, vol. 4, no. 1, p. 17, 2015. [Online]. Available: https://doi.org/10.14421/biomedich.2015.41.17-24

[77] Y. Zhang, X. Liao, F. Chen, J. Wu, and X. Hu, "Isolation, identification, and color characterization of cyanidin-3-glucoside and cyanidin-3-sophoroside from red raspberry," *European Food Research and Technology*, vol. 226, no. 3, pp. 395–403, 2008. [Online]. Available: https://doi.org/10.1007/s00217-006-0550-3

[78] F. Qu, N. Gong, S. Wang, Y. Gao, C. Sun, W. Fang, and Z. Men, "Effect of pH on fluorescence and absorption of aggregates of chlorophyll a and carotenoids," Dyes and Pigments, vol. 173, p. 107975, 2020. [Online]. Available: https://doi.org/10.1016/j.dyepig.2019.107975

[79] G. F. C. Mejica, Y. Unpaprom, D. Balakrishnan, N. Dussadee, S. Buochareon, and R. Ramaraj, "Anthocyanin pigment-based dye-sensitized solar cells with improved pH-dependent photovoltaic properties," *Sustainable Energy Technologies and Assessments*, vol. 51, Sept. 2021. [Online]. Available: https://doi.org/10.1016/j.seta.2022.101971

[80] E. Rápó and S. Tonk, "Factors affecting synthetic dye adsorption; desorption studies: A review of results from the last five years (2017–2021)," *Molecules*, vol. 26, no. 17, 2021. [Online]. Available: https://doi.org/10.3390/molecules26175419

[81] D. D. Pratiwi, F. Nurosyid, A. Supriyanto, and R. Suryana, "Optical properties of natural dyes on the dye-sensitized solar cells (DSSC) performance," *Journal of Physics: Conference Series*, vol. 776, no. 1, p. 012007, 2016. [Online]. Available: https://doi.org/10.1088/1742-6596/776/1/012007

[82] J. Tauc, R. Grigobovici, and A. Vancu, "Optical Properties and Electronic Structure of Amorphous Germanium," in *De Gruyter*, 1966, pp. 709–720.

[Online]. Available: https://doi.org/doi:10.1515/9783112492505-079
[83] S. Suyitno, T. J. Saputra, A. Supriyanto, and Z. Arifin, "Stability and efficiency of dye-sensitized solar cells based on papaya-leaf dye," *Spectrochimica Acta - Part A: Molecular and Biomolecular Spectroscopy*, vol. 148, pp. 99–104, 2015. [Online]. Available: https://doi.org/10.1016/j.saa.2015.03.107
[84] J. Conradie, "Effective dyes for DSSCs–Important experimental and calculated parameters," *Energy Nexus*, vol. 13, p. 100282, 2024. [Online]. Available: https://doi.org/10.1016/j.nexus.2024.100282
[85] E. C. Prima, *Electron transfer investigation of modified anthocyanin solar cells using spectroscopy and density functional theory methods*, Institut Teknologi Bandung, 2016.
[86] P. Faqih, N. A. Aini, and Z. Mardhiyah, "Effect of concentration of red dragon fruit (*Hylocereus costaricensis*) peels extract as a dye of dye-sensitized solar cell (DSSC) on DSSC efficiency," in *Proc. Int. Conf. on Science and Applied Science (ICSAS)*, 2019. [Online]. Available: https://doi.org/10.1063/1.5141733
[87] F. Kabir *et al.*, "Instability of dye-sensitized solar cells using natural dyes and approaches to improving stability – An overview," *Sustainable Energy Technol. Assess.*, vol. 52, p. 102196, 2022. [Online]. Available: https://doi.org/10.1016/j.seta.2022.102196
[88] P. Setiarso, R. V. Harsono, and N. Kusumawati, "Fabrication of dye sensitized solar cell (DSSC) using combination of dyes extracted from Curcuma (Curcuma xanthorrhiza) rhizome and Binahong (Anredera cordifolia) leaf with treatment in pH of the extraction," *Indonesian Journal of Chemistry*, vol. 23, no. 4, pp. 924–936, 2023. [Online]. Available: https://doi.org/10.22146/ijc.77860
[89] S. Mahalingam and H. Abdullah, "Electron transport study of indium oxide as photoanode in DSSCs: A review," *Renewable and Sustainable Energy Reviews*, vol. 63, pp. 245–255, 2016. [Online]. Available: https://doi.org/10.1016/j.rser.2016.05.067
[90] M. M. H. Bhuiyan *et al.*, "Effect of combination of natural dyes and the blocking layer on the performance of DSSC," in *Dye-Sensitized Solar Cells*, A. M. Elseman, Ed. London, U.K.: IntechOpen, 2021, ch. 15. [Online]. Available: https://doi.org/10.5772/intechopen.94760
[91] C. Y. Chien and B. D. Hsu, "Optimization of the dye-sensitized solar cell with anthocyanin as photosensitizer," *Solar Energy*, vol. 98, pp. 203–211, 2013. [Online]. Available: https://doi.org/10.1016/j.solener.2013.09.035

Andhy Setiawan, photograph and biography not available at the time of publication.

Sandi Muhammad Roziq, photograph and biography not available at the time of publication.

Eka Cahya Prima, photograph and biography not available at the time of publication.

Agus Danawan, photograph and biography not available at the time of publication.

Endi Suhendi, photograph and biography not available at the time of publication.

Semuel Unwakoly, photograph and biography not available at the time of publication.